Electronic Theses and Dissertations, 2004-2019

2008

Numerical Modeling Of Wave Propagation In Nonlinear Photonic Crystal Fiber

Md. Kaisar Khan
University of Central Florida

Showcase of Text, Archives, Research & Scholarship

NUMERICAL MODELING OF WAVE PROPAGATION IN NONLINEAR PHOTONIC CRYSTAL FIBER

by

MD. KAISAR RASHID KHAN
B. Sc. Eng. Bangladesh Institute of Technology, 1995
M. Eng. Bangladesh University of Engineering and Technology, 1997
M. S. The University of Texas at El Paso, 2001

A dissertation submitted in partial fulfillment of the requirements
for the degree of Doctor of Philosophy
in the School of Electrical Engineering and Computer Science
in the College of Engineering & Computer Science
at the University of Central Florida,
Orlando, Florida

Summer Term
2008

Major Professor: Thomas X. Wu

In the name of Allah most beneficial and merciful

Dedicated to:

My Lord Allah, who create and sustain me,

My guide Mohammad (peace be upon him), who shows me how to worship Allah and

My parent Sajeda Khanam and Md. Abdur Rahman Khan, who bring me in this world

ABSTRACT

In this dissertation, we propose numerical techniques to explain physical phenomenon of nonlinear photonic crystal fiber (PCF). We explain novel physical effects occurred in PCF subjected to very short duration pulses including soliton. To overcome the limitations in the analytical formulation for PCF, an accurate and efficient numerical analysis is required to explain both linear and nonlinear physical characteristics. A vector finite element based model was developed to precisely synthesize the guided modes in order to evaluate coupling coefficients, nonlinear coefficient and higher order dispersions of PCFs. This finite element model (FEM) is capable of evaluating coupling length of directional coupler implemented in dual core PCF, which was supported by existing experimental results. We used the parameters extracted from FEM in higher order coupled nonlinear Schrödinger equation (HCNLSE) to model short duration pulses including soliton propagation through the PCF. Split-step Fourier Method (SSFM) was used to solve HCNLSE.

Recently, reported experimental work reveals that the dual core PCF behaves like a nonlinear switch and also it initiates continuum generation which could be used as a broadband source for wavelength division multiplexing (WDM). These physical effects could not be explained by the existing analytical formulae such as the one used for the regular fiber. In PCF the electromagnetic wave encounters periodic changes of material that demand a numerical solution in both linear and nonlinear domain for better accuracy. Our numerical approach is capable of explaining switching and some of the spectral features found in the experiment with much higher degree of design freedom. Numerical results can also be used to further guide experiments and theoretical modeling.

ACKNOWLEDGMENTS

will always remain in our memory because we begin our conjugal life here. Thanks to Japa's family too for their encouragements.

As always we take refuge to the mercy of Allah particularly at the time of challenges. Me and Japa thank our lord Allah when he blessed us with his miracle (our daughter Jaiyana)! On the other hand, I become patient and ask for his mercy when my mother passed away in 2005 while I was in this program.

My father and my siblings are always in my memory and I am trying my best to fulfill their dream of being a successful person. My family is my inspiration.

TABLE OF CONTENTS

vi

LIST OF FIGURES

LIST OF ACRONYMS/ABBREVIATIONS

Definition of Acronym	Acronym
Boundary element method	(BEM)
Beam propagation method	(BPM)
Continuous Wave	(CW)
Coupled nonlinear Schrödinger equations	(CNLSE)
Cross phase modulation	(XPM)
Dense wavelength division multiplexing	(DWDM)
Finite difference time domain	(FDTD)
Finite element method	(FEM)
Fourier Transform	(FFT)
Four Wave Mixing	(FWM)
Group velocity dispersion	(GVD)
Higher Order Coupled Nonlinear Schrödinger equation	(HCNLSE)
Holey fibers	(HF)
Inter modal dispersion	(IMD)
Internet Protocol	(IP)
Inverse Fourier Transform	(IFT)
Multiplexer-demultiplexer	(MUX-DEMUX)
Nonlinear directional coupler	(NLDC)
Nonlinear Schrödinger equation	(NLSE)
Photonic bandgap	(PBG)

Photonic crystal fiber   (PCF)

Self phase modulation   (SPM)

Split-step Fourier method   (SSFM)

Stimulated Raman scattering   (SRS)

Stimulated Brillouin scattering   (SBS)

Third order dispersion   (TOD)

Transverse Magnetic   (TM)

Transverse Electric   (TE)

Wavelength division multiplexing   (WDM)

CHAPTER 1:   INTRODUCTION

1.1   Introduction

Nonlinear behaviors of waveguide structure have been studied in electromagnetic and optics for the past few decades [1-9]. Theoretical as well as the experimental works open the door of opportunities to invent new devices in microwave and optics area. One of the recent trends of optical waveguide research and development work is governed by the requirement of different device structures subjected to nonlinear effect [7, 10-11]. Dielectric material shows nonlinear effects due to intensity dependent change of refractive index and stimulated inelastic scattering [1-7]. Vector wave equation derived from the Maxwell equation represents the electromagnetic wave propagation through the waveguide [3-5]. Depending on the structure and material properties, numerical solution of electromagnetic wave equations requires modification [8-12]. If the system becomes nonlinear then extra attention is required. Because in that case material's refractive index itself changed due to higher field intensity [1-2]. When these waveguides support short duration pulses the dispersion and nonlinearity plays together. Moreover for coupled waveguide structures, coupling characteristics also need to be found in order to understand the pulse propagation properties [1, 4, 10]. When the input pulse is intense the nonlinearity is triggered in these waveguide that causes switching and new frequency generations due to multiple nonlinear processes [1-7]. In order to understand these processes we need to find all of the above mentioned properties (dispersion, coupling etc) for a wide frequency/wavelength region. This was the primary motivation of the present research.

Recently researchers have showed intense interests on a special type of optical waveguide called photonic crystal fiber (PCF) because of its engineerable dispersion, coupling and nonlinear properties [13-17]. These make PCF a suitable candidate for many applications which could not be possible or difficult by using regular optical fiber. Recent theoretical and experimental works reveal many possible nonlinear processes in PCF which could be used for numerous applications [13-14, 17-20]. A careful and accurate linear and nonlinear modeling is necessary to explain many of the above mentioned properties. Analytical formulation similar like the one used for the regular optical fiber is not sufficient as the structure posses a periodic changes of material [17-21]. A numerical approach is necessary to accurately analyze the waveguide modes. There are some numerical methods already available with their pros and cons. Finite difference time domain (FDTD) method, beam propagation method (BPM), boundary element method (BEM), and finite element method (FEM) have been used to model PCFs [13,22-26]. Among these methods, the FEM is famous for its accuracy because it evaluates local functions in small discretized elements [12-13, 26].

In the present research we have developed a vector finite element model to solve wave equation in order to evaluate propagating modes of dielectric waveguide. The method is robust and it avoids having spurious/non physical solution [12]. Before analyzing the PCF structure using the above mentioned model, we have evaluated dispersion coefficient for both rectangular and circular shaped waveguide and compared with the existing analytical results for the validity check of the model [8-9].

To consider nonlinearity we changed the refractive index of the dielectric medium due to the variation of electric field intensity at the respective elements. Our finite element method

2

(FEM) solver provides us the electric field along with the wave vector which we used to update the refractive index. Starting with single nonlinear waveguide structure, our research is later extended to the nonlinear coupled optical waveguide structures. The coupling characteristics of coupled nonlinear waveguide are also presented in later chapters.

When these waveguides support short duration pulses numerous interesting physical effects were observed both in the linear and nonlinear domain. Nonlinear Schrödinger Equation (NLSE) is usually used to model the pulse propagation through the waveguide [1]. This propagation equation is further modified based on the waveguide and pulse properties. Split Step Fourier Method (SSFM) was used to solve the pulse propagation equations. In the later chapters of this dissertation, results are presented to explain linear and nonlinear physical effects due to short duration pulse (including soliton) propagation through the optical waveguide.

1.2   Numerical Methods in Electromagnetics

Numerical analysis is the study of algorithms for the problems of continuous mathematics [27-28]. In practical mathematical calculations it does not seek exact answers, because exact answers are impossible to obtain in practice. Instead, much of numerical analysis is concerned with obtaining approximate solutions while maintaining reasonable bounds on errors [9,12,27]. Before the advent of modern computers numerical methods often depended on hand interpolation in a large printed tables [27-28]. Nowadays computers can calculate the required functions. The interpolation algorithms may be used as part of the software for solving both ordinary and partial differential equations [9,12,27]. Partial differential equations involved in electromagnetics problem are solved by first discretizing the equation and bringing it into a finite-dimensional

subspace [9,12]. This can be done by a finite element method, a finite difference method, or a finite volume method [27]. The theoretical justification of these methods often involves theorems from functional analysis [9,12]. This reduces the problem to the solution of an algebraic equation which is easier to calculate [12]. The numerical methods used for our nonlinear waveguide analysis are FEM for EM analysis and beam propagation method (BPM) for optical pulses propagation.

1.3   Numerical Methods Used for Nonlinear Optical Waveguide Analysis

1.3.1   Finite Element Method

Finite Element Method is a numerical method that proposes an approximate solution to the boundary value problem [9, 12]. Starting from 1940's the FEM has a history of solving boundary value problem in mathematics and physics [12, 27-28]. This method was initially focused on air craft design. Later it was adopted by the civil engineers for structural design [12, 29]. Today the method is extended to many other areas of physics and engineering. An approximate solution to any complex engineering problem can be reached by subdividing the problem into smaller more manageable (finite) elements [9, 12, 27]. Using finite elements, solving complex partial differential equations that describe the behavior of certain structures can be reduced to a set of linear equations that can be easily solved using the standard techniques of matrix algebra [12].

FEM is a unique numerical method which addresses problems in areas of physics and engineering that include fluid mechanics, mechanics of materials, chemical reactions,

semiconductor devices, electromagnetics, optics, quantum mechanics, acoustics etc. The key features of FEM are [9, 12, 27-29]

1. Piecewise approximation of continuous field gives good precision even with the simple approximating functions.

2. Using computational time and resources we can improve the precision just by increasing the number of elements.

3. FEM analysis approximates the element of small sizes and different shapes. This eases the application of complex shape of different materials and different boundary conditions.

4. It covers both linear and nonlinear problems.

5. Local approximation generates sparse system of equation that helps to solve problem having large number of modal unknown.

FEM substitute the continuous function by a number of discrete sub domains. Unknown function in the sub domain is represented by simple interpolation functions with unknown coefficient [9, 12]. That approximates the original boundary value system by a finite number of unknown coefficients. Ritz variation or Galerkin procedure convert the boundary value problem to a finite number of algebraic equations [12]. Solving these algebraic equations led us to find the unknown coefficients. With the sparsity of the coefficient matrices, FEM exhibits pleasing characteristic of computational economy in numerical modeling [12]. The success of FEM in electromagnetics can be largely attributed to their great versatility and flexibility, which allow the treatment of geometrically complex structures with inhomogeneous, anisotropic or even nonlinear materials [27-28].

In summary the boundary value problem solution using FEM should have the following steps [9, 12, 27-29]:

1. Discretization of the domain

2. Proper selection of the interpolation function

3. Formulation of system of algebraic equations using Ritz or Galerkin method

4. Solution of the system of algebraic equations

1.3.2 Split-Step Fourier Method

The Split-Step Fourier Method (SSFM) is a pseudo-spectral numerical method used to solve nonlinear partial differential equations such as NLSE [1,10]. The name arises for two reasons. First, the method relies on computing the solution in small steps, and treating the linear and the nonlinear steps separately. Second, it is necessary to Fourier transform back and forth because the linear step is made in the frequency domain while the nonlinear step is made in the time domain [1,10]. This method is used in the field of light pulse propagation in optical fibers, where the interaction of linear and nonlinear mechanisms makes it difficult to find general analytical solutions. However, the split-step method provides a numerical solution to the problem. Use of Fast Fourier Transform (FFT) improves the speed of the computation [30]. In general NLSE describes the dispersion and nonlinearity which act together in optical waveguide. For optical beam propagation the NLSE is expressed as

$$i\frac{\partial \phi}{\partial z} + \frac{\partial^2 \phi}{\partial x^2} + \frac{\partial^2 \phi}{\partial y^2} + V(x,y)\phi + |\phi|^2 \phi = 0 \tag{1.1}$$

The first term is the evolution term, second and third terms are for diffraction, fourth term is for the optical potential under initial excitation and the last term is for the nonlinearity [10]. The above initial value problem can not be solved analytically in the general case. Therefore the use of numerical methods is inevitable [1, 10]. NLSE for the pulse propagation is similar to equation (1.1) except diffraction in spatial domain is replaced by the dispersion in time domain [10].

The main idea of SSFM is to find approximate solutions of NLSE by assuming that the diffraction and nonlinear effects act independently [10]. Here we split the propagation of the field in two steps: one for diffraction only and one for nonlinear propagation only. Moreover, we calculate the linearly propagating field by working in the Fourier space [10, 30]. By applying this technique over many small steps, we can numerically find the solution of Eq. (1.1) for every small step in the distance z.

Working in the Fourier space for the linear part of the problem is better for two reasons: (a) the operators become a scalar quantity, and (b) FFT algorithm is very fast [10, 30]. A NLSE system can be written by separating the linear and nonlinear part as [1, 10]

$$\frac{\partial A}{\partial t} = (L+N)A \qquad (1.2)$$

where L and N are the linear and nonlinear parts of the equation. The solution over a short time interval τ can be written in the form

$$A(t+\tau, x) = \exp(\tau_L)\exp(\tau_N)A(t, x) \qquad (1.3)$$

where the linear operator in the NLSE system acting on a spatial field *B(t,x)* is written in Fourier space as

$$\exp(\tau_L)B(t,x) = F^{-1}\exp(ik^2\tau)FB(t,x) \tag{1.4}$$

where F denotes the Fourier Transform (FT), F^{-1} denotes the Inverse Fourier Transform(IFT), and k is the spatial frequency.

Computation of A over time interval τ has been done ☐ infour steps:

Step1 (nonlinear step): Compute $A_1 = \exp(\tau N)\,A(t, x)$ (by finite differences).

Step 2 (forward FT): Perform the forward FT on A_1: $A_2 = F(A_1)$

Step3 (linear step): Compute $A_3 = exp(\tau L)A_2$.

Step 4 (backward FT): Perform the backward FT on A_3: $A(\tau + t) = F^{-1}A_3$.

For numerical approximation of this algorithm, the potential A is discretized in the form $A_l = A(lh)$ for $l = 0, \ldots , N-1$, where h is the space-step and N is the total number of spatial mesh points.

The split-step approximation is accurate for small distances [10]. So we are going to solve equation (1.1) for a small distance, under the assumption that the operator B does not depend on z. We did this approximation before deriving the NLSE, when we superimposed the diffraction and Self Phase Modulation (SPM) effects.

Again in brief the key features of SSFM are [1, 10, 30-31]

1. Split-step (linear & nonlinear) method

2. Derivatives in the frequency domain

3. Multiplication in the time domain

4. Easily applied to modifications of the NLSE

1.4   Outline of the Dissertation

In this dissertation we will focus on the study of the wave propagation through nonlinear optical waveguide using numerical techniques. Specific waveguide structure will be considered in this study is the dual core photonic crystal fiber (PCF). The study intends to come up with the results to explain necessary physics of these devices.

Chapter One is the general introduction of the numerical methods used here to study the optical waveguide and nonlinear pulse propagation through it. Vector FEM was used to evaluate dispersion, coupling and nonlinear parameters of the wave guide and SSFM is used for analyzing pulse propagation through it.

Chapter Two of this dissertation talks about the finite element formulation of the wave equation. A vector formulation of wave equation and its solution procedure based on vector FEM has been presented in this chapter. We present numerical examples of dielectric waveguide and compare our results with already reported analytical results for validation check of the model.

Chapter Three discusses the general introduction of PCF working as an optical waveguide, its advantages over regular optical fiber and its applications. Dispersion and coupling characteristics of dual core PCF has also been presented. Design effort is demonstrated in this chapter to show that the geometry can be adjusted to achieve desired linear and nonlinear characteristics.

Nonlinear phenomena observed in optical waveguide, are described in Chapter Four of this dissertation. Nonlinear phase shift (due to Kerr nonlinearity) and scattering are the major nonlinear effects discussed there. Issues related to soliton propagation and its application in optical communication is also reviewed.

9

In Chapter Five we discuss the nonlinear directional coupler implemented in PCF to support short pulses including soliton. Formulation of NLSE has been shown to model the pulse propagation through the waveguide. Later we use SSFM to solve the propagation equation. NLSE has been modified in order to incorporate the issues related to femto second pulse propagation.

Chapter Six shows the switching characteristics of PCF coupler. Soliton switching occurred in dual core PCF is presented there. We show our design effort to adjust PCF parameters so that it can support soliton switching.

Multi frequency generation and determination of its underline causes have been discussed in Chapter Seven. Both time and frequency domain nonlinear analysis revealed the nature of generating other frequencies. It also help us to understand the existence of other nonlinear process observed in the recently conducted experiment such as four wave mixing and third harmonic generation.

Chapter Eight briefly discusses the conclusion of the available results and more importantly give an overview of future guideline for theoretical and experimental research related to these types of nonlinear waveguides. The present work already explain some of the physical effects such as linear coupling between two core of PCF, switching in PCF coupler, soliton wave propagation and also higher frequency generation at intense input power. The study also differentiate between the existing theoretical results and the experiment which lead us to search for appropriate phase matched condition so that we can under stand other nonlinear effects.

CHAPTER 2:   FINITE ELEMENT FORMULATION

2.1   Introduction to FEM Formulation

We initiate our numerical formulation with vector wave equation and solve for different propagation modes. An edge element based finite element model was developed for that. Careful attention was given to avoid spurious or nonphysical solution of this waveguide modal analysis. After that we extended the developed model for periodic and coupled structure to numerically evaluate dispersion and coupling characteristics. Intended results guide the direction of research concerning linear and nonlinear wave propagation. In this chapter we discuss the method of studying electro magnetic wave propagation in wave guide using FEM.

2.2   Vector FEM: A Review

The vector finite element method is used to compute the mode spectrum of electromagnetic waveguides with arbitrary cross section [12, 32]. We encounter some serious problem in node based element analysis which was the primary motivation of finding new edge based element analysis. Some of the limitations of nodal analysis are [12, 27,32]

1. The occurrence of nonphysical or spurious solutions, which is generally attributed to lack of enforcement of divergence condition.

2. The inconvenience of imposing boundary conditions at material interfaces and as well as in conducting surfaces.

3. Difficulties in treating conducting and dielectric edges and corners due to field singularities associated with these structures.

The edge element based analysis eliminates the disadvantages of the scalar finite element approach of having undesired spurious modes or non-physical solutions and easy implementation of boundary conditions at material interfaces [12]. This approach uses vector basis that assign degrees of freedom to the edges rather than to the nodes of the elements. Although this kind of element was first mentioned in 60's by Whitney, they were not implemented in electromagnetics until 80's [33]. Nedlec discusses the construction of tetrahedral and bricks element [34]. Hano introduces rectangular edge elements for the analysis of dielectric-loaded wave-guide [35]. Mur and De hoop considered the problem of Electro Magnetic (EM) field in inhomogeneous media [36]. Effort was made to analyze optical waveguide [10, 37]. Depending on the structure and application we need to choose the element's shape and sizes as well as implementing proper boundary conditions [12].

2.3 Vector FEM Formulation for Waveguide Modal Analysis

The first and foremost requirement of any FEM is to have a good meshing. That means we need to discretize the continuous spectrum. Also we enclose the structure with an electrical wall as shown in Figure 2.1.
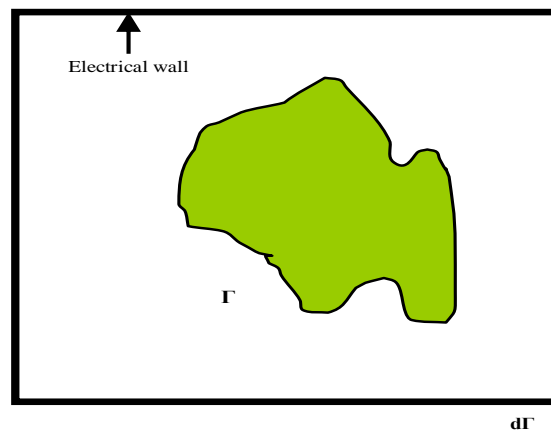
Figure 2.1 Arbitrary shaped waveguide with electrical wall

The vector finite element formulation can be illustrated by using either the electric field $\mathbf{E}$ or magnetic field $\mathbf{H}$ field; here we explain the case for the $\mathbf{E}$ field, which is the same for the $\mathbf{H}$ field. Wave equation has its origin at the famous four set of Maxwell's equations [8, 12]. They are

$$\nabla \times \mathbf{E} = -\mu_0 \frac{\partial \mathbf{H}}{\partial t} \tag{2.1}$$

$$\nabla \times \mathbf{H} = \varepsilon_r \frac{\partial \mathbf{E}}{\partial t} \tag{2.2}$$

$$\nabla \cdot \varepsilon_r \mathbf{E} = 0 \tag{2.3}$$

$$\nabla \cdot \mathbf{H} = 0 \tag{2.4}$$

Where μ_r and ε_r are the permeability and permittivity of the material. After some simple derivation and using vector identity we have the vector wave equation for the $\mathbf{E}$ field which is given by

$$\nabla \times \left(\frac{1}{\mu_r} \nabla \times \mathbf{E} \right) - k_0^2 \varepsilon_r \mathbf{E} = 0 \tag{2.5}$$

The transverse and longitudinal components are separated and can be written as

$$\nabla_t \times \left(\frac{1}{\mu_r} \nabla_t \times \mathbf{E}_t \right) + \frac{1}{\mu_r} \left(k_z^2 \nabla_t E_z + k_z^2 \mathbf{E}_t \right) = k_0^2 \varepsilon_r \mathbf{E}_t \tag{2.6}$$

$$-\frac{1}{\mu_r} \left[\nabla_t \cdot \left(\nabla_t E_z + \mathbf{E}_t \right) \right] = k_0^2 \varepsilon_r E_z \tag{2.7}$$

Here, k_z is the longitudinal propagation constants.

To apply Galerkin's method to the above equations, we multiply equation (2.6) with the testing function $\mathbf{T}_t$ and equation (2.7) with the testing function T_z and integrate both the equations over the cross section of the structure Γ [12, 32]; then these two equations become

$$\iint_{\Gamma}\left[\mathbf{T}_t \cdot \nabla_t \times \left(\frac{1}{\mu_r}\nabla_t \times \mathbf{E}_t\right) + \frac{k_z^2}{\mu_r}\left(\mathbf{T}_t \cdot \nabla_t E_z + \mathbf{T}_t \cdot \mathbf{E}_t\right)\right]ds = k_0^2 \varepsilon_r \iint_{\Gamma} \mathbf{T}_t \cdot \mathbf{E}_t \, ds \qquad (2.8)$$

$$-\frac{1}{\mu_r}\iint_{\Gamma} T_z \left[\nabla_t \cdot \left(\nabla_t E_z + \mathbf{E}_t\right)\right]ds = k_0^2 \varepsilon_r \iint_{\Gamma} T_z E_z \, ds \qquad (2.9)$$

Using the vector identities; we can write the weak form of the above equations as

$$\frac{1}{\mu_r}\iint_{\Gamma}\left[\left(\nabla_t \times \mathbf{T}_t\right)\cdot\left(\nabla_t \times \mathbf{E}_t\right) + \left(k_z^2 \mathbf{T}_t \cdot \nabla E_z + k_z^2 \mathbf{T}_t \cdot \mathbf{E}_t\right)\right]ds$$
$$= k_0^2 \varepsilon_r \iint_{\Gamma} \mathbf{T}_t \cdot \mathbf{E}_t \, ds - \frac{1}{\mu_r}\int_{d\Gamma} \mathbf{T}_t \cdot \left(\hat{n} \times \nabla \times \mathbf{E}_t\right)dl \qquad (2.10)$$

$$-\frac{1}{\mu_r}\iint_{\Gamma}\left(\nabla_t T_z \cdot \nabla_t E_z + \nabla_t T_z \cdot \mathbf{E}_t\right)ds = k_0^2 \varepsilon_r \iint_{\Gamma} T_z E_z \, ds + \frac{1}{\mu_r}\int_{d\Gamma}\left(T_z \frac{\partial E_z}{\partial n} + T_z \hat{n} \cdot \mathbf{E}_t\right)dl \quad (2.11)$$

If the structure boundary $d\Gamma$ in Figure 2.1 is assumed to be perfectly conducting, then $\mathbf{T}_t$ = 0 and T_z = 0 on $d\Gamma$. Therefore the line integrals on the right hand side of equations (2.10) and (2.11) can be neglected. Multiplying equation (2.11) with k_z^2 for the sake of symmetry and rearranging the equations we have

$$\frac{1}{\mu_r}\iint_{\Gamma}\left(\nabla_t \times \mathbf{T}_t\right)\cdot\left(\nabla_t \times \mathbf{E}_t\right)ds - k_0^2 \varepsilon_r \iint_{\Gamma} \mathbf{T}_t \cdot \mathbf{E}_t \, ds = -\frac{k_z^2}{\mu_r}\left(\iint_{\Gamma} \mathbf{T}_t \cdot \nabla E_z \, ds + \iint_{\Gamma} \mathbf{T}_t \cdot \mathbf{E}_t \, ds\right) \quad (2.12)$$

$$\frac{k_z^2}{\mu_r}\iint_{\Gamma} \nabla_t T_z \cdot \nabla_t E_z \, ds + \frac{k_z^2}{\mu_r}\iint_{\Gamma} \nabla_t T_z \cdot \mathbf{E}_t \, ds = k_0^2 k_z^2 \varepsilon_r \iint_{\Gamma} T_z E_z \, ds \qquad (2.13)$$

Since the vector Helmholtz equation is divided into two parts as equations (2.6) and (2.7), vector-based tangential edge elements, shown in Figure 2.2(a), can be used to approximate the

transverse fields, and nodal-based elements, shown in Figure 2.2(b), can be used to approximate the longitudinal component.
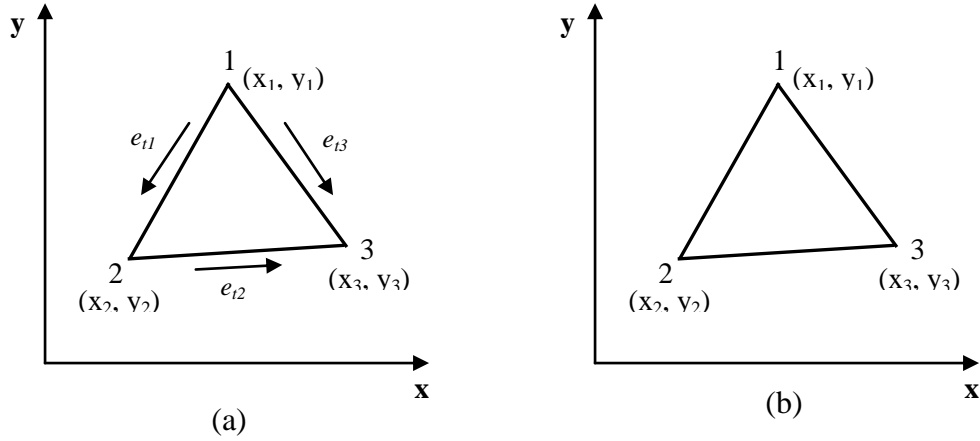
Figure 2.2 Configuration of (a) tangential edge elements (b) node elements

For a single triangular element shown in the above figure the transverse electric field can be expressed as a superposition of edge elements. The edge elements permit a constant tangential component of the basis function along one triangular edge while simultaneously allowing a zero tangential component along the other two edges [12, 32, 38]. Three such functions overlapping each triangular element provides the complete expansion, that is

$$\mathbf{E}_t = \sum_{m=1}^{3} e_{tm} \mathbf{W}_{tm} \tag{2.14}$$

Where m indicates the m-th edge of the triangle and $\mathbf{W}_{tm}$ is the edge element for edge m given by

$$\mathbf{W}_{tm} = L_{tm}\left(\alpha_i \nabla_t \alpha_j - \alpha_j \nabla_t \alpha_i\right) \tag{2.15}$$

L_{tm} is the length of edge m connecting nodes i and j and α_i is the first-order shape function associated with nodes 1, 2 and 3 given by

$$\alpha_i = \frac{1}{2A}(a_i + b_i x + c_i y)$$ (2.16)

and a_i, b_i, and c_i are given by

$$a_i = x_j y_k - x_k y_j$$ (2.17)

$$b_i = y_j - y_k$$ (2.18)

$$c_i = x_k - x_j$$ (2.19)

Where i, j, and k are cyclical and A is given by

$$A = \frac{1}{2}\begin{vmatrix} 1 & x_1 & y_1 \\ 1 & x_2 & y_2 \\ 1 & x_3 & y_3 \end{vmatrix}$$ (2.20)

The longitudinal component is written as

$$E_z = \sum_{i=1}^{3} e_{zi}\alpha_i$$ (2.21)

Where i indicate the ith node and α_i is given by equation (2.16). The testing functions $\boldsymbol{T}_t$ and T_z are chosen to be the same as the corresponding basis function in equations (2.12) and (2.13); that is $\boldsymbol{T}_t = \mathbf{W}_{tm}$ and $T_z = \alpha_i$ [2,10].

Substituting equations (2.14) and (2.15) into equations (2.12) and (2.13), respectively, integrating over a single triangular element, and interchanging the integration and summation gives

$$\frac{1}{\mu_r}\sum_{m=1}^{3}\iint_{\Delta}(\nabla_t \times \mathbf{W}_{tm})\cdot(\nabla_t \times \mathbf{W}_{tn})e_{tm}\,ds - k_0^2\sum_{m=1}^{3}\varepsilon_r\iint_{\Delta}(\mathbf{W}_{tm}\cdot\mathbf{W}_{tn})e_{tm}\,ds$$
$$= -k_z^2\left[\frac{1}{\mu_r}\sum_{m=1}^{3}\iint_{\Delta}(\mathbf{W}_{tm}\cdot\nabla\alpha_j)e_{zj}\,ds + \frac{1}{\mu_r}\sum_{m=1}^{3}\iint_{\Delta}(\mathbf{W}_{tm}\cdot\mathbf{W}_{tn})e_{tm}\,ds\right]$$ (2.22)

(n=1,2,3; j=1,2,3)

$$\frac{k_z^2}{\mu_r}\sum_{i=1}^{3}\iint_{\Delta}\left(\nabla\alpha_i\cdot\nabla\alpha_j\right)e_{zi}\,ds+\frac{k_z^2}{\mu_r}\sum_{i=1}^{3}\iint_{\Delta}\left(\nabla\alpha_i\cdot\mathbf{W}_{tm}\right)e_{tn}\,ds=k_z^2\sum_{i=1}^{3}k_0^2\varepsilon_r\iint_{\Delta}\alpha_i\alpha_j e_{zi}\,ds \qquad (2.23)$$

(j=1,2,3; n=1,2,3)

where the subscripts of α and $\mathbf{W}_t$ indicate node number and edge numbers respectively. Equations (2.22) and (2.23) can be written in matrix form as,

$$\begin{bmatrix} S_{e(tt)} & 0 \\ 0 & 0 \end{bmatrix}\begin{bmatrix} e_t \\ e_z \end{bmatrix}=-k_z^2\begin{bmatrix} T_{e(tt)} & T_{e(tz)} \\ T_{e(zt)} & T_{e(zz)} \end{bmatrix}\begin{bmatrix} e_t \\ e_z \end{bmatrix} \qquad (2.24)$$

The elements of the above matrices are given by

$$S_{e(tt)}=\frac{1}{\mu_r}\iint_{\Delta}\left(\nabla_t\times\mathbf{W}_{tm}\right)\cdot\left(\nabla_t\times\mathbf{W}_{tn}\right)ds-k_0^2\varepsilon_r\iint_{\Delta}\left(\mathbf{W}_{tm}\cdot\mathbf{W}_{tn}\right)ds \qquad (2.25)$$

$$T_{e(tt)}=\frac{1}{\mu_r}\iint_{\Delta}\left(\mathbf{W}_{tm}\cdot\mathbf{W}_{tn}\right)ds \qquad (2.26)$$

$$T_{e(tz)}=\frac{1}{\mu_r}\iint_{\Delta}\left(\mathbf{W}_{tm}\cdot\nabla\alpha_j\right)ds \qquad (2.27)$$

$$T_{e(zt)}=\frac{1}{\mu_r}\iint_{\Delta}\left(\nabla\alpha_i\cdot\mathbf{W}_{tn}\right)ds \qquad (2.28)$$

$$T_{e(zz)}=\frac{1}{\mu_r}\iint_{\Delta}\left(\nabla\alpha_i\cdot\nabla\alpha_j\right)ds-k_0^2\varepsilon_r\iint_{\Delta}\alpha_i\alpha_j\,ds \qquad (2.29)$$

These element matrices are assembled over all the triangular elements in the cross section of the structure to obtain a global eigenvalue equation [32],

$$\begin{bmatrix} S_{tt} & 0 \\ 0 & 0 \end{bmatrix}\begin{bmatrix} e_t \\ e_z \end{bmatrix}=-k_z^2\begin{bmatrix} T_{tt} & T_{tz} \\ T_{zt} & T_{zz} \end{bmatrix}\begin{bmatrix} e_t \\ e_z \end{bmatrix} \qquad (2.30)$$

Solving the above equation yields the eigenvalues or the longitudinal propagation constants k_z, from which the effective refractive index n_e is obtained using the relation [12, 29, 32]

$$n_e = \left(\frac{k_z}{k_0}\right) \tag{2.31}$$

2.4   Power Flow through the Waveguide

In order to investigate the nonlinear effect of waveguide it is necessary to accurately evaluate the power flowing through the waveguide. Because nonlinear effect demonstrated in the waveguide is due to the power intensity dependent change of the refractive index. The total power input to the waveguide is the sum of power dissipated in all triangular elements. In our FEM model we calculate the wave vector as well as it gives us the nodal and edge component of electric field from that we evaluate electric field in an element E as

$$\mathbf{E} = \mathbf{E}_t + \hat{\mathbf{z}}E_z \tag{2.32}$$

Here $\mathbf{E}_t$ is the transverse component electric field vector and E_z is electric field component at the direction of propagation as shown in equations (2.14) and (2.21). Power flow (Pointing Vector) in the direction of propagation (z direction) is evaluated by the curl operation of electric and complex conjugate of the magnetic field in transverse direction as shown in the following equation

$$\begin{aligned} P &= \tfrac{1}{2}\mathrm{Re}[\iint (\mathbf{E}_t \times \mathbf{H}_t^{*}) \cdot \hat{\mathbf{z}}\,dxdy] \\ &= \tfrac{1}{2}\tfrac{k_z}{\omega\mu}\iint |Et|^2\,dxdy \end{aligned} \tag{2.33}$$

2.5   Nonlinear Perturbation and Eigenmodes of Optical Waveguide

For small power the above mentioned modal analysis is reasonable. But at higher input power the waveguide refractive index changes due to nonlinearity [1-5]. Strong electric field due to higher input power is the major contributor to the nonlinear perturbation to the material. For Kerr like nonlinear material, the electric field dependent dielectric constant is given by [1-2, 38]

$$\tilde{\varepsilon}(\omega, |E|^2) = \varepsilon(\omega) + 2n(\omega)n_2|E|^2 \tag{2.34}$$

Here n_2 is the nonlinear index coefficient. For silica fiber n_2 yield a value in the range 2.2-3.4 x10^{-20} m^2/W. E is the normalized electric field for a given input power. As the n_2 is positive in silica glass it increases the refractive index with the wave intensity, leading to convergences of light rays from neighborhood sites towards the region of higher amplitude. This in turn further increases the refractive index and leads to more light convergence, resulting in a self-focusing of the wave at this location [1-2].

After evaluating linear (without perturbation) eigenvalue for the even and odd modes we adjusted the dielectric constant using equation (2.34) and then solve the equation (2.30) again. This iterative process continues until the eigenmode converged. In order to provide the high degree of accuracy for eigenvalue calculation, we let the iteration running until it converges to a very small preset error.

2.6   Validity Check of the Developed FEM Code

The solution of equation (2.30) provides us the propagation constant of the waveguide in the direction of wave propagation. FEM based customized computer codes (both in MATLAB and in FORTRAN) have been written for this purpose. This program provides us the wave vector

along with the field profile of the waveguide. Before we move forward to analyze periodic PCF structure, we solve the above equations for simple rectangular as well as circular waveguide. We test the validity of our model by reproducing the numerical and also analytical results for dielectric waveguide presented in ref [8].

2.7   Mesh Generation for FEM Analysis

The accuracy of FEM heavily depends on the size and shape of the mesh and also approximation of local function. Better accuracy is achieved with small element size and higher degree polynomial [11, 39]. In real life problem, required accuracy is achieved by using fine meshes with large number of elements. The uniform subdivision of the domain using similar size elements perhaps the simplest type of meshing technique but clearly not the most efficient one [39]. For our numerical model we use MATLAB pdetool and use their adaptive meshing techniques (Delaunay triangulation) [39]. Our program extract node coordinate from the drawing, convert the local node number to global node number and also do the same thing for the edge number in order to assemble element matrix to system matrix. We also have to designate node and edges at the waveguide boundaries in order to apply proper boundary conditions. The tool is smart enough to generate optimized triangular elements to cover computation domain [39]. Accurate drawing of the PCF geometry is required to have symmetric mesh generation. Careful drawing of PCF geometry is also an essential requirement for investigating underline physics of this periodic structure. In the later chapters some dispersion and coupling results will show that they are dependent on PCF geometry. We also developed custom codes that will generate the PCF geometry. The code is flexible and can be modified easily for different PCF dimensions

20

without redrawing the structure again. This gives the designer the convenience as well as much higher degree of freedom.

The element size can be optimized by adjusting mesh parameter of the tool [39]. User can approximate higher order polynomial in the FEM program to incorporate curve boundary. Obviously extra computational cost and time will be added for higher order polynomial and more elements required for the fine meshing. Depending on the application user has to do tradeoff between the computational cost and accuracy.

CHAPTER 3: DISPERSION ANALYSIS OF PHOTONIC CRYSTAL FIBER

3.1 General Introduction of Optical Waveguide

Optical waveguides have been widely used in optical communications and drastically changed the world. Fiber optic cable and semiconductor laser cavities are common examples of optical waveguides. Optical waveguides consist of adjacent, optically transparent sections of material with different refractive indices. The section that transmits the light has a slightly higher refractive index, so that total internal reflection acts to guide the light within the medium [1, 8].

Present optical fiber technology maintains a careful trade-off between optical losses, optical nonlinearity, group–velocity dispersion and polarization effects [1, 13-14, 40]. Optical fiber loss is inherent in the raw material used to make the fiber which is silica glass (SiO_2) [1]. But nonlinearity and dispersion are strongly affected by the material's properties and can also be influenced by fiber design.

3.2 PCF a New Type of Optical Waveguide

Since early 80's the optical scientists discover that the ability to structure materials on the scale of the optical wavelength, will allow the development of new optical materials known as photonic crystals [40]. A new kind of fiber was proposed called photonic crystal fiber (PCF) [16]. It was also called as holey fiber, hole-assisted fiber or microstructured fiber [13, 41-43]. A PCF is an optical fiber which obtains its waveguide properties not from a spatially varying material composition but from an arrangement of very tiny and closely spaced air holes which go through the whole length of fiber [13, 16-17]. It is a regular morphological microstructure incorporated

into the material to radically alter its optical properties [13, 41]. It has a central region of pure silica (core) surrounded by air holes. Such air holes can be obtained by using a preform with (larger) holes, made by stacking capillary tubes (stacked tube technique) [13, 16-17]. Soft glasses and polymers (usually plastics) also allow the fabrication of preforms for photonic crystal fibers by extrusion [19,44]. There is a great variety of air hole arrangements, leading to PCFs with very different properties.

3.2.1 Photonic Bandgap Fibers

In PCF, a wavelength dependant effective volume average index difference between the defect regions will form the core, and the surrounding region which contains air holes, will be acting as the cladding [13]. This effective-index guidance does not necessarily depend on having a periodic array of holes. Even other arrangements could serve a similar function [13]. Another waveguide named photonic bandgap fiber (PBG fiber) was designed and fabricated [16-17, 41]. It has a totally different guiding mechanism, which is based on a photonic bandgap at the cladding region [41]. Because of the wavelength dependence of the refractive index between the core and cladding, the PBG fibers can also possess a complete photonic band gap. That means they let some wavelength to pass and block some wavelength depending on the size of the air holes relative to the period of the lattice [13, 41, 45]. The latter mechanism even allows guidance in a hollow core (i.e., in a low-index region). Such air-guiding hollow-core photonic crystal fibers (air core bandgap fibers) can have a very low nonlinearity and a high damage threshold [42]. They typically guide light only in a relatively narrow wavelength region with a width of e.g.

23

100-200 nm and can be used for pulse compression with high optical intensities, because most of the power propagates in the hollow core [1, 42].

3.2.2   Light Guiding in PCF

In the conventional fiber, light guided in the core when light in the core has higher value of propagation constant, k_z than that of the cladding. The largest value of k_z that can exist in an infinite homogeneous medium with refractive index n is $k_z = nk_0$, and all smaller values of propagation constant allowed. We derive propagation constant from our FEM. Either conventional homogeneous material or artificially fabricated photonic crystals are used to make PCF [1, 13].

Figure 3.1 shows the schematic of PCF core and cladding region. Light is guided in the core region due to higher effective refractive index in the core region. Here the diameter of the air hole in the cladding region is denoted by d and the distance between the centers of two air holes is called pitch Λ. We often change d and Λ to adjust PCF geometry for our numerical model.
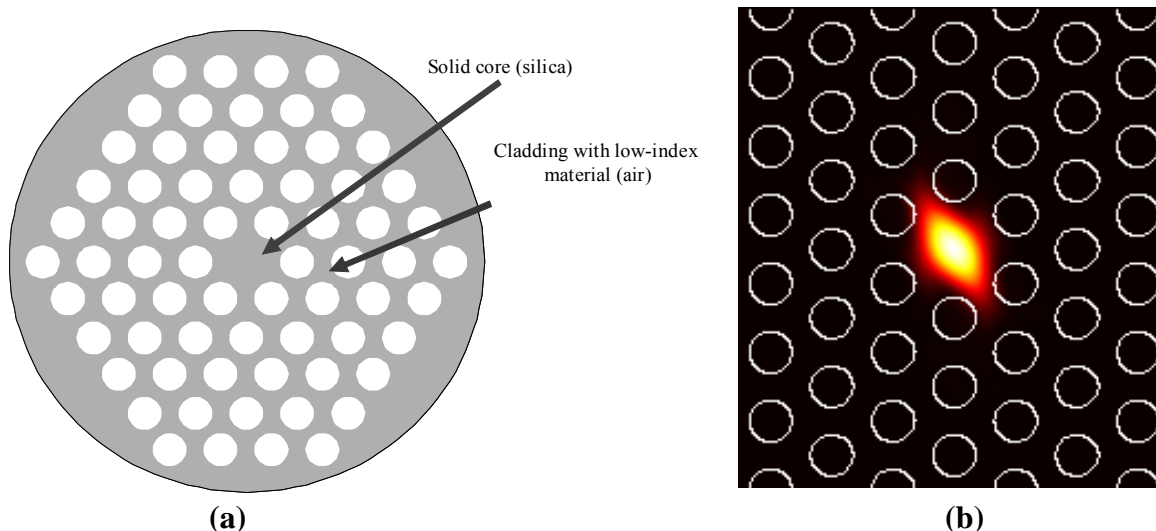
Figure 3.1 (a) PCF geometry: core and cladding (b) confined light in core area

A PCF is a periodic structure where propagation constant in the direction of propagation k_z varies with the wavelength. In our FEM model we evaluate the k_z as a function of wavelength λ. This is the single most important characteristics of PCF waveguide because it determines the shape and nature of the guided wave [1, 8, 13].

3.2.3   Achievable Properties of PCF by Geometry Design

PCFs with different designs of the air hole pattern can have very remarkable properties which are strongly dependent on the design details. Some of them are [46-49]

1. Very high numerical aperture of e.g. 0.6 or 0.7 of multimode fibers.

2. Endlessly single-mode guidance over very wide wavelength regions.

3. Low sensitivity to bend losses even for large mode areas.

4. Extremely small or extremely large mode areas than a conventional fiber, leading to very strong or weak optical nonlinearities.

5. The possibility to fill gases or liquids into the holes and make extremely strong birefringence for polarization-maintaining fibers.

6. Very unusual and engineerable chromatic dispersion properties, e.g. anomalous dispersion in the visible wavelength region.

7. Core-less end caps, fabricated simply by fusing the holes near the fiber end with a heat treatment (sealed end facets), allowing for higher mode areas at the fiber surface and thus a higher damage threshold.

8. The feasibility of multi-core designs, e.g. with a regular pattern of core structures in a single fiber, where there are some coupling between the cores.

3.2.4 Applications of PCF

The above mentioned unique properties make photonic crystal fibers very attractive for a wide range of applications. Some examples are [13, 46-52]:

1. Fiber lasers and amplifiers, including high-power devices, mode-locked fiber lasers, etc.

2. Nonlinear devices such as suppercontinum generation (frequency combs), Raman conversion, parametric amplification, or pulse compression is possible by using PCF because both weak and strong nonlinearity can be achieved in PCF by proper design.

3. Telecom components, such as dispersion controller, filter and all optical switches.

4. Fiber-optic sensors.

5. Application in quantum optics such as generation of correlated photon pairs, electromagnetically induced transparency, or guidance of cold atoms

Even though PCFs have been around for couple of years, the huge range of possible applications is far from being fully explored [13]. It is expected that this field will stay very lively for many years and give a lot of opportunities for further creative work, both concerning fiber designs and applications [13-16].

3.3   PCF Coupler

In a usual PCF, there is one defect in the central region and the light is guided along this defect. Recently, adjacent two defects were introduced into a PCF. It has been shown that it is possible to use the PCF as an optical fiber coupler [53]. These PCF couplers with adjacent two cores have possibility of realizing a multiplexer-demultiplexer (MUX-DEMUX).

We have studied dual core PCF and evaluated coupling characteristics using FEM [54-55]. Figure 3.2 shows schematic of a dual core PCF. Some dimension of PCF geometry such as d, and core separation C was adjusted to obtain the desired effect. To implement FEM we generated mesh using PDE tool to get the nodal and edge information.
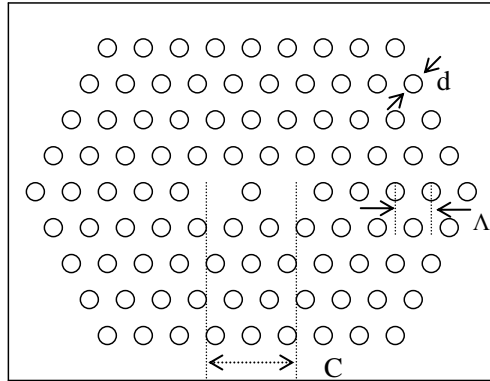
Figure 3.2 (a) Schematic cross section and (b) dimensions of dual core PCF

3.3.1 Effective Refractive Index Evaluation of PCF Coupler

Effective refractive index of PCF has been evaluated by using the formulae used in equation (2.30) in the previous chapter. Figure 3.3 shows the n_e with the wavelength. At short wavelength its change is more rapid than at longer wavelength. At short wavelength material dispersion is more prominent while at longer wavelength the waveguide dispersion starts to take over. That is the reason why the waveguide geometry shows their effect. As the air hole diameter d, increases the n_e also increases.
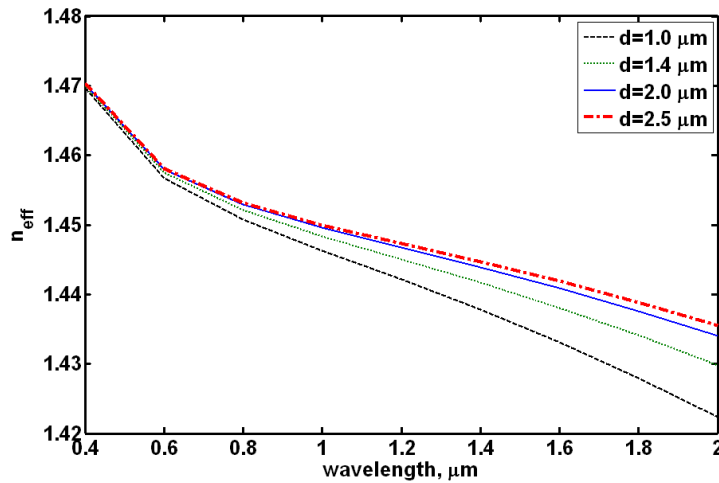
Figure 3.3 Effective refractive index of dual core PCF (d=1 μm, C=4 Λ and d/Λ=0.8)

3.3.2 Evaluation of Coupling Length of PCF Coupler

In brief optical power is exchanged between the coupled cores due to weak overlap of adjacent electric field. Here two simultaneously excited supper modes (even and odd modes) of the combined structure are supported by the two PCF cores [55]. Since wave vector for even mode k_{ze} and wave vector for odd mode k_{zo} are not same, they develop a relative phase difference in propagation. This phase difference which is responsible for periodic power transfer between two cores depends on the distance traveled by the wave and can be expressed as

$$\Psi(z) = (k_{ze} - k_{zo})z \tag{3.1}$$

Here light confined into one of the PCF core jumps to the other waveguide after propagating a distance known as coupling length Lc owing to the different propagation constants of the even and odd modes of the coupler shown in Figure 3.4. Coupling length Lc is determined by the following equation,

$$L_C = \frac{\pi}{k_{ze} - k_{zo}} \tag{3.2}$$

(a)   (b)
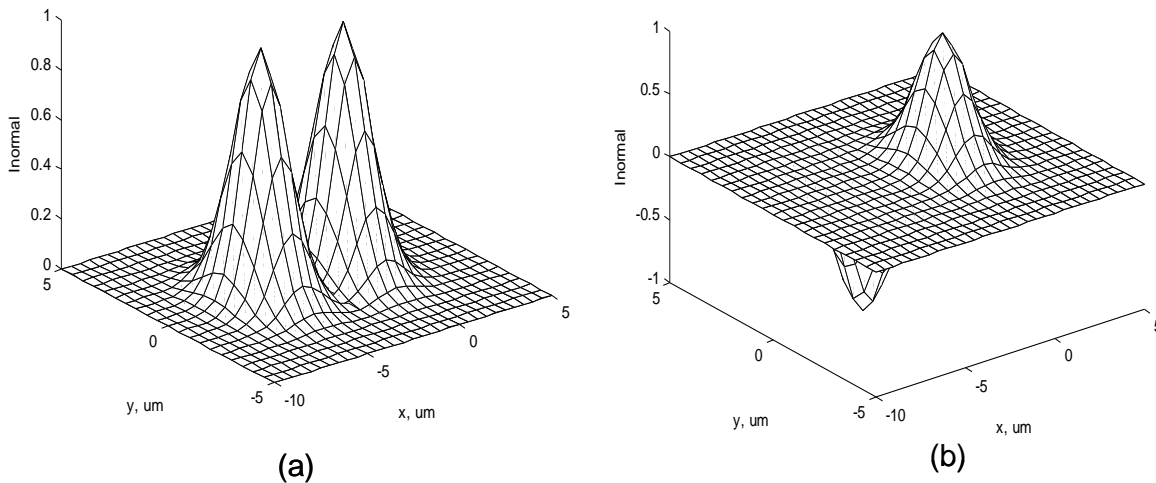
Figure 3.4 Intensity profile of the two distinct super modes: (a) even mode (b) odd mode

The effective refractive index for these two distinct super mode have been shown for the PCF coupler shows that their difference is very small at short wavelength and as the wavelength increases it shows their difference. Figure 3.5 shows the n_e f for the PCF coupler with d=1.0 μm, C=2Λ and d/Λ =0.7.

(a)   (b)
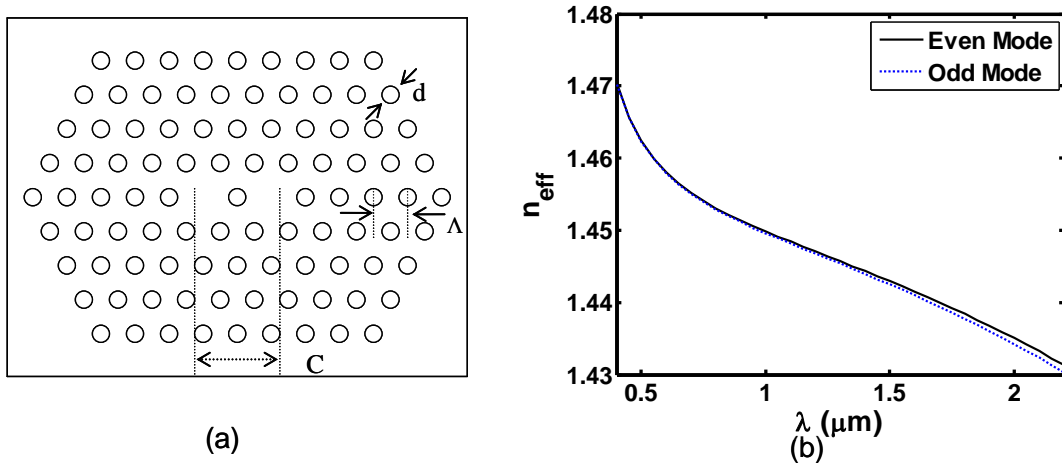
Figure 3.5 n_{eff} of even and odd super modes of PCF couplers (d=1.0 μm, C=2Λ and d/Λ =0.7)

It is shown from numerical results that it is possible to realize significantly short MUX-DEMUX PCFs, compared to the conventional optical fiber couplers. Figure 3.6 shows the wavelength dependency of Lc. It is observed that the coupling length decreases with the increase of wavelength at short wavelength and at longer wavelength (greater than 1.5 μm), there is a small change of Lc observed with wavelength.

(a)

(b)
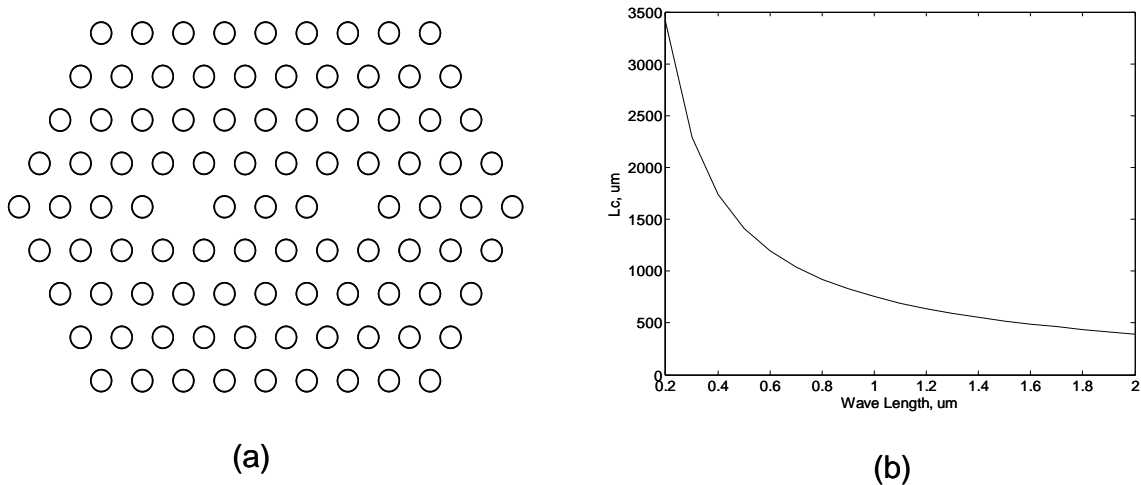
Figure 3.6 Coupling lengths of PCF couplers (d=0.8 **μ**m, C=4 Λ and d/Λ =0.7)

3.3.3 Effect of Material Dispersion on Coupling Length

In our FEM we considered ε_r of air hole in PCF as 1 and that of the silica glass is wavelength λ dependent which can be expressed by the following Sellmier expansion [1, 56]

$$\varepsilon_r(\lambda) = 1 + \sum_{n=1}^{3} \frac{A_n \lambda^2}{\lambda^2 - B_n} \tag{3.3}$$

A and *B* are the Selmeir coefficients. In case of silica glass these are [1]

A_1=0.69675; A_2=0.408218; A_3=0.890815 and B_1=0.0047701; B_2=0.0133777; B_3=98.02107 and

the wavelength λ is given in micro meter unit [1].

We include the wavelength dependent permittivity during the element analysis of the FEM. Inclusion of wavelength dependent material dispersion in our model makes it more realistic. We observe the effect of material dispersion on the coupling length of PCF, specifically at short wavelength where material dispersion is more prominent [55]. Figure 3.7 shows the coupling length L_C with the wavelength for d/Λ=0.9 [55]. A noticeable difference of *Lc* is observed at shorter wavelength when we consider wavelength dependant refractive index of silica instead of

31

assuming it constant (n=1.45). At a longer wavelength this difference is less because the material dispersion is not that prominent at that wavelength region. It is also shown from the numerical results that it is possible to realize significantly short (1mm~1cm) PCF coupler, compared to conventional optical fiber couplers [21, 54].
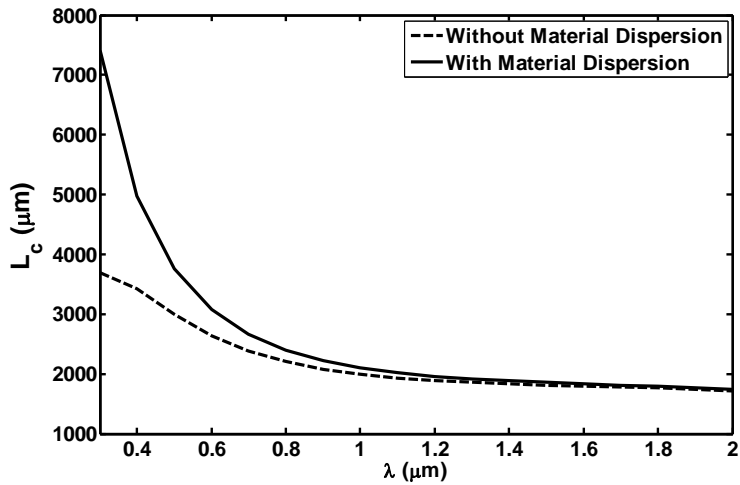
Figure 3.7 Effect of material dispersion on the coupling length of a dual core PCF (d=1.0 μm, C=4 Λ and d/Λ =0.9).

3.3.4   PCF Geometry and Coupling

Changing PCF dimensions (d, Λ or C) let the designer flexibility to manage the coupling length. Changing d and C by keeping d/Λ constant will change the effective refractive index n_e and also the coupling length. Even though the core separation decreases as d increases for a fixed d/Λ but we see an increase of coupling length Lc in Figure 3.8. This is because the deference of even and odd modes decreases as the d increases.
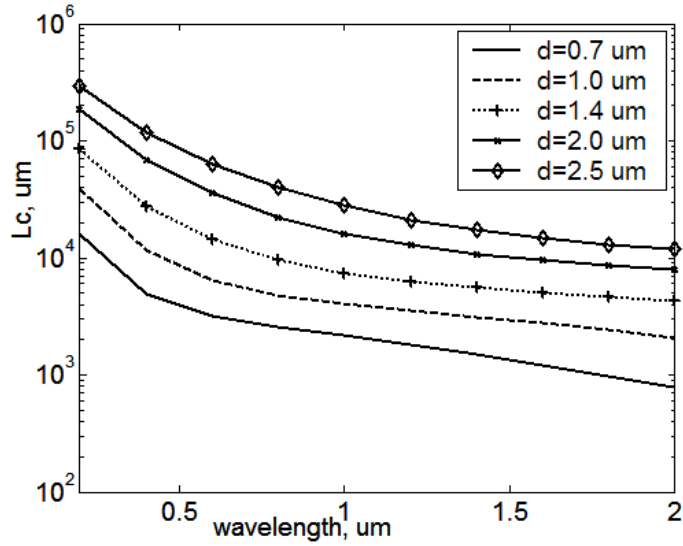
Figure 3.8 Comparison of coupling length of dual core PCF coupler (C=4 Λ, d/Λ=0.8)

Our next research objective was to observe the coupling length profile of the dual core PCF with same core size and a fixed core separation, but varying the d of those air holes which were placed in cladding region and also their d/Λ ratio. We kept d of those air holes that constitutes the core region fixed, in order to preserve the integrity of the cores. In our first designed PCF in Figure 3.9 (a) we consider C=4 μm, d=1.0 μm and d/Λ=0.4. In the second design in Figure 3.9 (b) we alternately changed the hole diameter in the cladding region (d_1=1.0 μm and d_2=1.5 μm). In the third design in Figure 3.9(c) we gradually increased the d (d_1=1.0 μm, d_2=1.25 μm, d_3=1.5 μm and d_4=1.75 μm). In all three PCF coupler we kept d/Λ ratio as 0.4. We wanted to know what will be the outcome if this ratio is changed. To see this we designed the fourth PCF coupler with d=1.0 um and d/Λ=0.7 shown in Figure 3.9 (d).
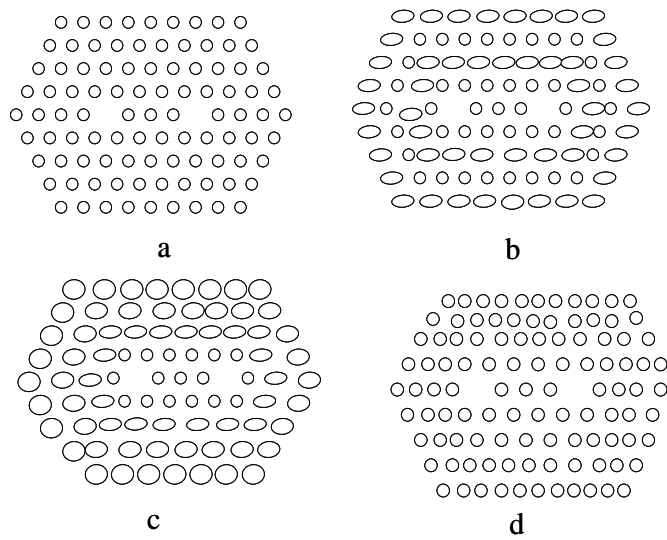
Figure 3.9 PCF Geometry: (a). PCF1 (b) PCF2 (c) PCF3 (d) PCF4

Figure 3.10 shows the coupling length of these four types of PCF coupler. *Lc* which is related to the difference of even and odd mode wave vector, shows a cross over around 1.1 μm and at longer wavelength for three types of PCF coupler with d/Λ=0.4. *Lc* values changes as the wavelength increases. As was expected *Lc* for the fourth PCF coupler with d/Λ=0.7 shows smaller value.
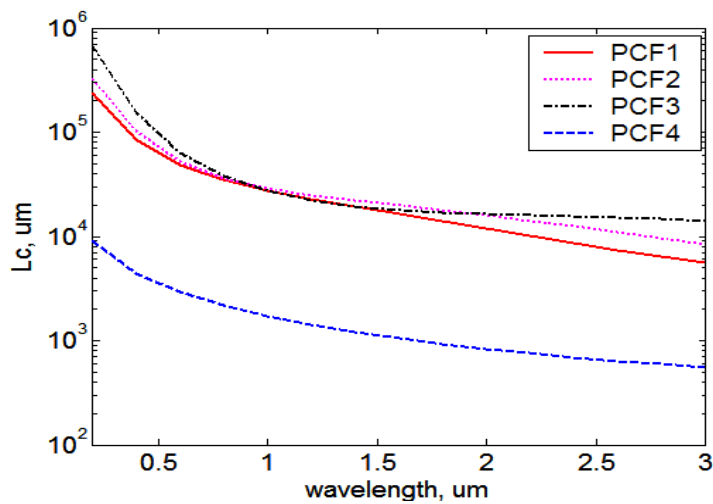
Figure 3.10 Comparison of Lc for the PCFs shown in Fig.3.9

3.4   Chromatic Dispersion in PCF

The main issue that limits transmission bitrate in optical fibers is dispersion. It is because generated impulses have a non-zero wide bandwidth and the medium have a refractive index that depends on resonance wavelength [57-59]. In other word when electromagnetic wave interacts with the bound electron of the dielectric materials, the medium response is frequency dependant and manifest through the change of refractive index n(ω). It is due to characteristic resonance frequency at which the bound electron oscillation of the dielectric medium absorbs the electromagnetic radiation [1, 59].

It is the dispersion of optical waveguide which is the most critical for short pulse propagation because the different spectral component associated with the pulse travel at different speed c/n(ω) [57-59].   If nonlinearity acts in the medium the combination of dispersion and nonlinearity will act together and shows novel physical phenomenon. Soliton pulse propagation through fiber is an example of such event. [1, 57-59]

Dispersion effects are accounted for by expanding the mode propagation constant k_z in Taylor series at a center frequency ω_0.

$$K_z(\omega) = \beta_0 + \beta_1(\omega - \omega_0) + \tfrac{1}{2}\beta_2(\omega - \omega_0)^2 + \ldots\ldots\ldots\ldots \tag{3.4}$$

Here

$$\beta_k = \left(\frac{d^k k_z}{d\omega^k}\right)_{\omega = \omega_0} \tag{3.5}$$

Second derivative of k_z with respect to ω is called β_2. It is the dispersion of the group velocity and responsible for pulse broadening [57-60]. This phenomenon is called the group velocity dispersion (GVD).

When pulse is send through the optical waveguide, it behaves differently for the sign of β_2. For normal dispersion regimes (wavelengths where $\beta_2 > 0$) high frequency component of optical pulse (blue shifted) travel slower than the low frequency component (red shifted) [1, 59]. Opposite action happens for the anomalous dispersion regime (wavelengths where $\beta_2 < 0$). In this wavelength range the fiber supports solitons by balancing dispersion and nonlinearities [1]. We will discus this phenomenon later in this dissertation.

3.4.1 Dispersion Evaluation of Dual Core PCF using FEM

From our FEM we evaluated the wave vector and effective refractive index n_e of the even and odd super mode with the frequency and then took the derivatives [55]. Figure 3.10 shows the frequency response of the waveguide's effective refractive index n_e. Figure 3.11 shows the β_2 which shows change of sign around 1.2 μm.
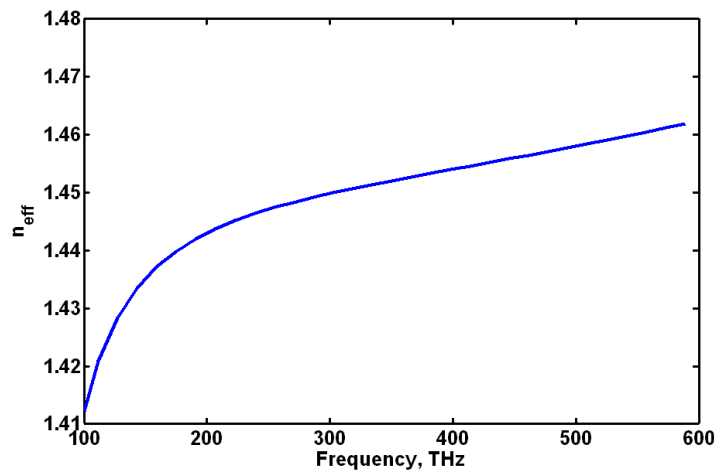
Figure 3.11 Effective refractive index of PCF coupler (d=1.0 μm, C=5 μm and d/Λ =0.4).
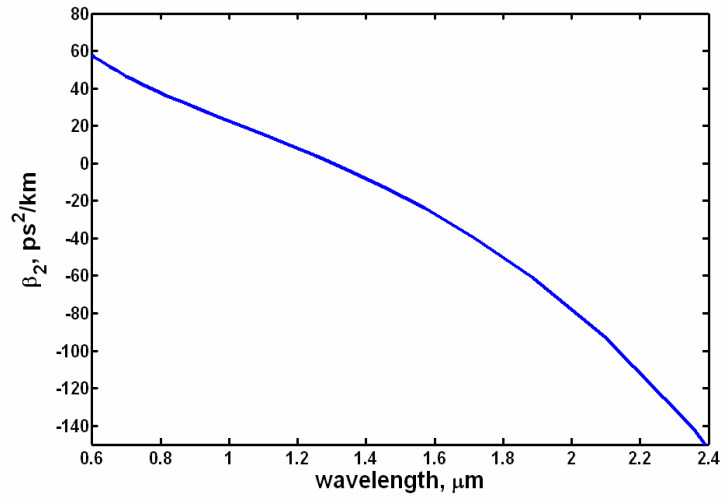
Figure 3.12 β_2 of dual core PCF (d=1.0 μm, C=5 μm and d/Λ =0.4).

Another parameter D which is commonly used in optical fiber literature in place of β_2 is related to β_2 by the relation in equation (3.5). Figure 3.13 shows D for the same PCF with d=1.0 μm, C=5 μm and d/Λ =0.4.

$$D = (\frac{d\beta_1}{d\lambda}) = -\frac{2\pi c}{\lambda^2} \beta_2 \qquad (3.5)$$
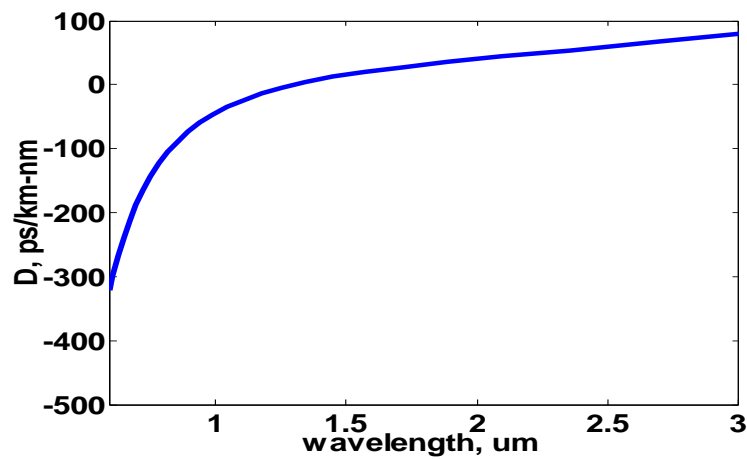
Figure 3.13 D of dual core PCF (d=1.0 μm, C=5 μm and d/Λ =0.4).

Another higher order dispersion parameter is β_3. It is also known as the third order dispersion (TOD) term as it is the third derivative of k_z with respect to ω. This term appears for very short pulses (< 1 ps) and can distort the pulse in both linear and nonlinear regimes [57-61]. Around zero dispersion ($\beta_2=0$) wavelength, inclusion of β_3 term is necessary [1]. When we analyze the pulse propagation through optical waveguide, k_z and its higher order derivatives determine the pulse broadening, changing of direction in the trailing and rising end of the pulses, pulse break up etc. Figure 3.14-15 show the subsequent higher order dispersion parameters for that PCF. From the figure a sharp change of slope is observed for β_3 and β_4 at longer wavelength. Value of β_4 is relatively small and can generally be ignored for pico or < 100 femto second pulse treatment. But for femto second pulses that generate higher frequencies, we need to incorporate these terms for pulse propagation modeling. This issue will be further discussed in Chapter 6 and 7 again.
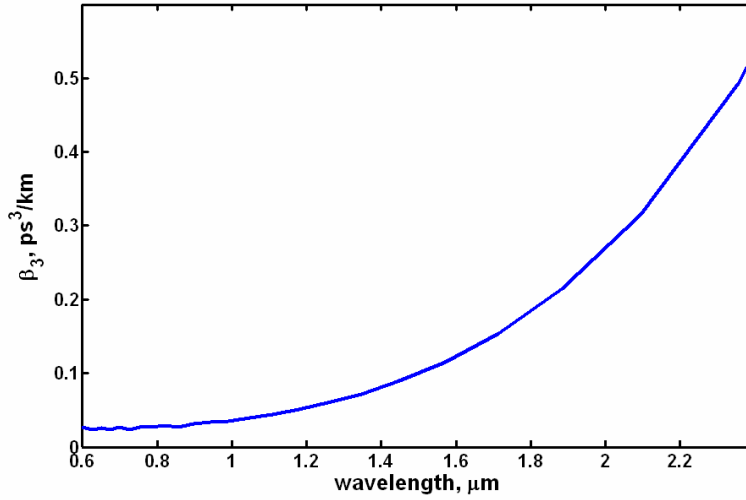
Figure 3.14 β_3 of dual core PCF (d=1.0 μm, C=5 μm and d/Λ =0.4).
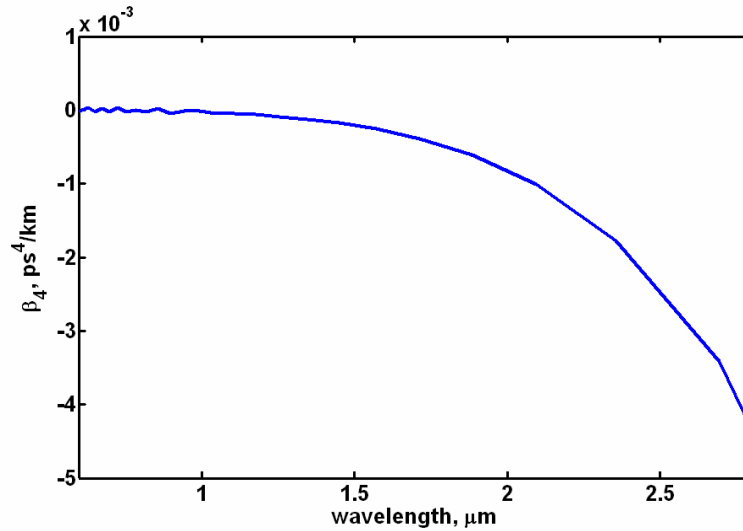
Figure 3.15 β_4 of dual core PCF (d=1.0 μm, C=5 μm and d/Λ =0.4).

3.4.2 PCF Design and Adjusting Dispersion

Dispersion can also be managed by changing PCF dimensions such as d, Λ or C [62-63]. Keeping Λ fixed and varying the d/Λ shifts the λ_d. From Fig. 3.16, it is observed that the λ_d shifts toward shorter wavelengths as d/Λ increases for a four ring PCF coupler with Λ =3.0 μm and C=4 Λ. For the similar PCF coupler with Λ =2.5 μm we found similar trend in λ_d shifting in

Figure 3.17, except values of λ_d s are little longer now. For a fixed Λ, decreasing d/Λ also decreases the air hole diameter d that eventually causes the electromagnetic wave to interact more with silica than the air. That it is why PCF demonstrates more waveguide dispersion at a larger d/Λ [55]. We only observed this at longer wavelengths because the waveguide dispersion is prominent at this wavelength region.
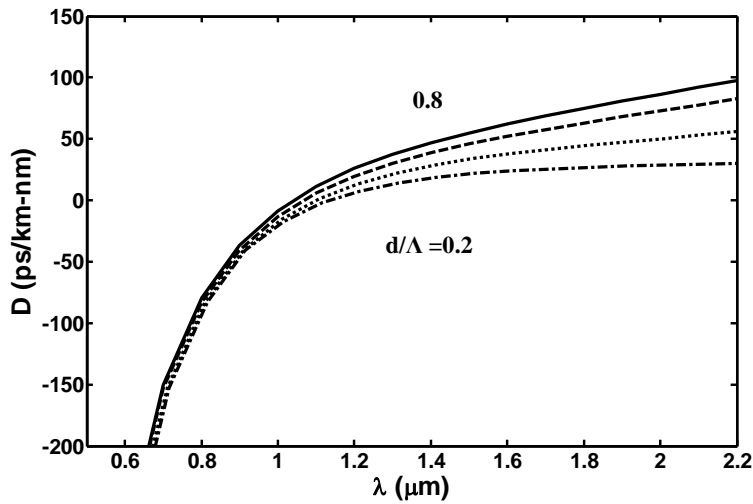
Figure 3.16 Comparison of GVD for the even super mode in four ring dual core PCFs with variable d (C=4 Λ, Λ=3.0 μm)
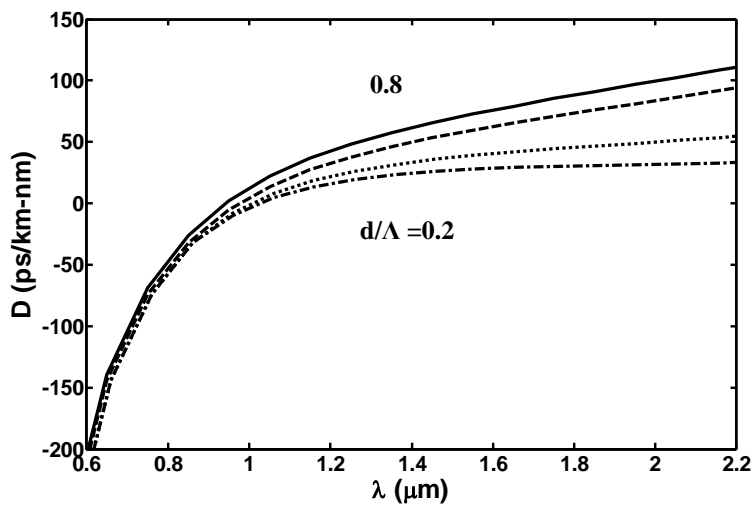
Figure 3.17 Comparison of GVD for the even super mode in four ring dual core PCFs with variable d (C=4 Λ, Λ=2.5 μm)

40

CHAPTER 4: WAVE PROPAGATION IN NONLINEAR OPTICAL WAVEGUIDE

4.1 Nonlinearity in Optical Waveguide

Like other dielectric the response of optical waveguide material to light is nonlinear for intense electromagnetic field [1]. It is due to the anharmonic motion of bound electron under the influence of applied field. As a result the total polarization induced by the electric dipole is not linear. The general formula for this nonlinear polarization relation is [1-7]

$$P = \varepsilon_o (\chi^{(1)}.E + \chi^{(2)}.EE + \chi^{(3)}.EEE......) \qquad (4.1)$$

Here permittivity depends on $\chi^{(j)}$ (j=1,2,3...) is the j th order susceptibility. $\chi^{(j)}$ is the tensor of rank j+1. $\chi^{(1)}$ is called the linear susceptibility and is the most dominant. Second order susceptibility $\chi^{(2)}$ is responsible for nonlinear effects like second harmonic generation or sum frequency generation [1-7]. It is present only in the media with lack of inversion symmetry at the molecular level. SiO_2 is symmetric that is the reason that the silica glass fiber does not show second order nonlinear effects [1-4].

4.1.1 Nonlinear Kerr Effect and Third Order Susceptibility

The Kerr effect is the effect of an instantaneously occurring nonlinear response that causes the change of refractive index. A nonlinear interaction of light in a medium with an instantaneous response, related to the nonlinear electronic polarization [1, 6]. This nonlinear optical effect occurred when intense light propagates in crystals, glasses and even in other media such as gases [2-6]. Its physical origin is a nonlinear polarization generated in the medium, which itself modifies the propagation properties of the light. Most of the nonlinear effects in

41

optical fiber are originated from the intensity dependent refractive index which can be expressed by the following relation [1]

$$\tilde{n}(\omega, |E|^2) = n(\omega) + n_2 |E|^2 \qquad (4.2)$$

This relation is well demonstrated in electromagnetics and optics and known as Kerr nonlinear effect. Here n_2 is the nonlinear index coefficient related to the third order susceptibility $\chi^{(3)}$ with the following relation:

$$n_2 = \frac{3}{8n(\omega)} \mathrm{Re}(\chi^3_{xxxx}) \qquad (4.3)$$

The n_2 value of a medium can be measured e.g. with the z-scan technique [1,6]. For silica fiber n_2 yield a value in the range 2.2-3.4 $\times 10^{-20}$ m^2/W [1-6]. This value is small compared to most other nonlinear material. In spite of the intrinsically small value of n_2 for silica fiber, nonlinear effect can be observed in single mode or PCF structure due to very small spot size and relatively low loss [1]. For soft glasses and particularly for semiconductors, n_2 can be much higher, because it strongly depends on the band gap energy. The nonlinearity is also often negative for photon energies above roughly 70% of the band gap energy. This is also known as self-defocusing nonlinearity [2-5]. Chalcogenide-glass fiber exhibits a measured n_2 of 4.2 $\times 10^{-18}$ m^2/W and is very promising in nonlinear optics [1, 60]. It is important to note here that many low order nonlinear effects such as third harmonic generation, four wave mixing and nonlinear refraction is dependent on the third order susceptibility $\chi^{(3)}$ [1-6].

The time and frequency dependent refractive index change leads to self-phase modulation and Kerr lensing, for different overlapping light beams also to cross-phase modulation. The

description of the Kerr effect via an intensity-dependent refractive index is actually based on an approximation that, it is valid for light with a small optical bandwidth [2-5]. For rather short and broadband pulses, a deviation from this simple behavior can be observed, which is called self-steepening [1]. It reduces the velocity with which the peak of the pulse propagates (i.e., it reduces the group velocity) and thus leads to an increasing slope of the trailing part of the pulse [1]. This effect is relevant e.g. for suppercontinum generation. Furthermore, the strength of the Kerr effect is known to saturate at very high optical intensities. [38].

4.1.2   Nonlinear Phase Shift

Optical field experiences a self induced phase shift while propagating through optical fibers. Magnitude of the phase shift is

$$\phi = \tilde{n} k_0 L = n k_0 L + n_2 |E|^2 k_0 L \tag{4.4}$$

where $k_0 = 2\pi/\lambda$ and L is the fiber length. The second term of above equation is nonlinear phase induced due to self phase modulation (SPM). SPM is responsible for spectral broadening for the ultra short pulses and formation of soliton in the anomalous dispersion regime of fiber ($\beta_2 < 0$) [1]. β_2 is the second-order dispersion or group velocity dispersion parameter . For standard silica fiber β_2 is 50 ps^2/km at visible region and -20 ps^2/km in ~1500 nm. [1, 59]

On the other hand cross phase modulation (XPM) is the nonlinear phase shift of an optical field with frequency (ω_1) induced by another field having a different polarization, frequency (ω_2) or direction. The nonlinear phase shift due to cross phase modulation can be expressed as the following

$$\phi_{NL} = n_2 (|E_1|^2 + 2|E_2|^2) k_0 L \tag{4.5}$$

The first term is the SPM and the second term is XPM.

4.1.3 Inelastic Nonlinear Effects

The nonlinear effect related to third order susceptibility $\chi^{(3)}$ is elastic in the sense that no energy is exchanged between the electromagnetic field and the medium [1]. On the contrary, the other class of nonlinear effect exchanges energy between electric field and the dielectric media. Two known phenomenon in this type are; stimulated Raman Scattering (SRS) and Stimulated Brillouin Scattering (SBS). Optical phonon (vibration of lattice) participates in SRS while acoustic phonon participates in SBS [1-7].

When light is scattered from a molecule, most photons are Rayleigh scattered which is elastically scattered where the scattered photons have the same energy and wavelength as that of the incident photons [1-4]. A photon in the incident field is annihilated to create a photon at a lower frequency and a phonon with right energy and the momentum to conserve energy and momentum. [1] A small fraction of the scattered light $(1/10^6)$ is scattered by an excitation having a frequency lower than, the frequency of the incident photons.

Indian physicist Chandrasekhara Venkata Raman published his work on the "Molecular Diffraction of Light", the first of a series of investigations with his collaborators which ultimately led to his discovery (in 1928) of the radiation effect which bears his name. Raman received the Nobel Prize in 1930 for his work on the scattering of light. Raman amplification can be obtained by using SRS, which actually is a combination between a Raman process with stimulated emission [1-4,64]. However, the process requires significant power and thus imposes

more stringent limits on the material. The amplification band can be up to 100 nm broad, depending on the availability of allowed photon states [1].

On the other hand, Brillouin scattering is an interaction of light photons with acoustic or vibrational quanta (phonons), with magnetic spin waves (magnons), or with other low frequency quasiparticles interacting with light. This is an inelastic scattering process in which a phonon or magnon is either created (Stokes process) or annihilated (anti-Stokes process) [1-6,64-65]. For intense beams (e.g. laser light) travelling through optical fiber, the variations in the electric field of the beam itself may produce acoustic vibrations in the medium via electrostriction. The beam may undergo Brillouin scattering from these vibrations, usually in opposite direction to the incoming beam. In optical waveguide supporting forward wave only SRS is observed because SRS presents in both forward and backward wave on the other hand SBS present for backward wave only [1].

4.2   Soliton Pulses

Soliton was first reported by Scott Russell in 1834 when he observed undistorted heap of water propagated couple of kilometers through the canal [1]. That solitary wave was formed due to sudden stop of a moving boat. He tracked down that wave on a horse back [1, 66-67]. However that wave properties was not completely understood until the inverse scattering method was developed [68]. The term soliton was coined in 1965 to reflect the particle like nature of that solitary wave that remains undistorted even after mutual collision [69]. Since then solitons have been studied in many branches of physics including optics [66-67, 70-71]. Use of soliton in optical communication was first suggested in 1973 [72]. The soliton pulses propagating in the

optical waveguide maintain same shape after traveling long distances [1]. Soliton forms in an optical fiber as a result of interplay between dispersion and nonlinearity. For unchirped soliton pulses it can be symbolized by the following hyperbolic secant function [1, 73]

$$q_1(0, \tau) = \sum_{k=0}^{N} \sqrt{P_0} \, \text{sech}[(\tau - k\tau_B)/\tau_0] \exp(j\phi) \tag{4.6}$$

Here P_0=Normalized Incident Power, τ_B =separation between adjacent bit, τ_0=1/e half width of pulse intensity, N is the soliton number (for fundamental soliton N=1) and φ=Z/2 is the phase of the pulse propagated which is a linear function of distance Z. Figure 4.1 shows two soliton pulses propagating through an optical waveguide. As shown in the figure the pulse remains undistorted as it propagates. It is due to delicate balance between the dispersion and the power of the pulse.

(a)

(b)
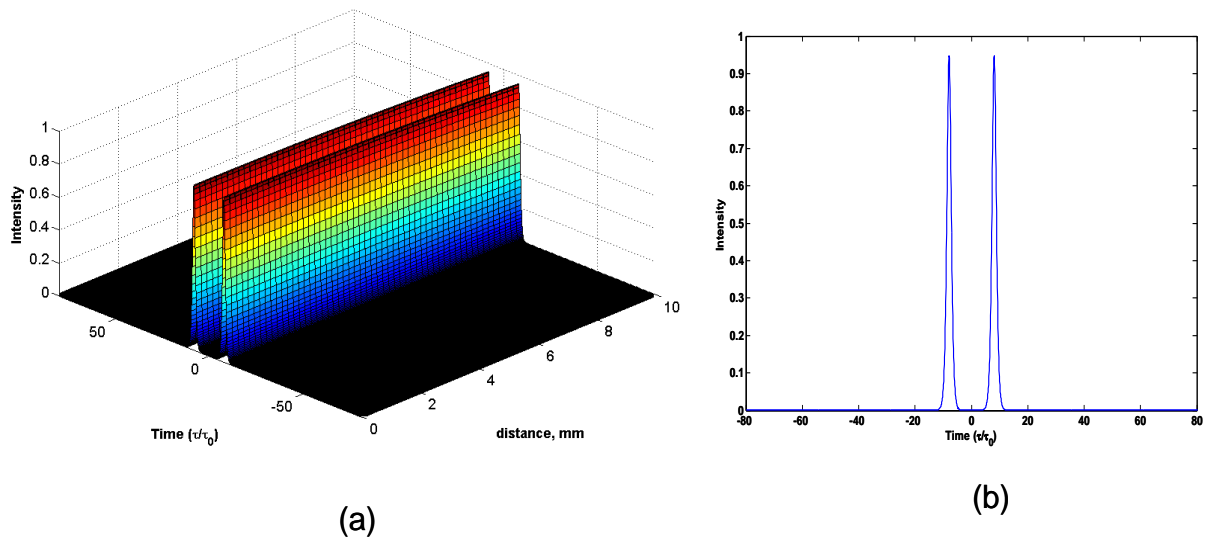
Figure 4.1 Soliton pulses propagation (a) 3D view (b) 2D view at the receiving end of the waveguide

4.3   Solitons in Fiber Optic Communication: A Literature Review

Much experimentation has been done using solitons in fiber optics applications. Solitons inherent stability make long-distance transmission possible without the use of repeaters, and could potentially double transmission capacity as well [57-59]. In 1973, Akira Hasegawa of AT&T Bell Labs was the first to suggest that solitons could exist in optical fibers, due to a balance between self-phase modulation and anomalous dispersion [72]. He also proposed the idea of a soliton-based transmission system to increase performance of telecommunications [67]. Solitons in a fiber optic system are described by the Manakov equations [67, 70-71]. In 1987, P. Emplit, et. al., from the Universities of Brussels and Limoges, made the first experimental observation of the propagation of a dark soliton, in an optical fiber [74]. In 1988, Linn Mollenauer and his team transmitted soliton pulses over 4,000 kilometers using Raman effect [75].

In 1991, a Bell Labs research team transmitted error-free 2.5 gigabits per second solitons over 14,000 kilometers, using erbium optical fiber amplifiers (spliced-in segments of optical fiber containing the rare earth element erbium). Pump lasers, coupled to the optical amplifiers, activate the erbium, which energizes the light pulses. In 1998, Thierry Georges and his team at France Télécom R&D Center, combining optical solitons of different wavelengths (WDM), demonstrated a data transmission of 1 terabit per second. For some reasons, it is possible to observe both positive and negative solitons in optic fibre. However, usually only positive solitons are observed for water wave [74-76].

CHAPTER 5: PULSE PROPAGATION THROUGH PCF

5.1 Introduction of Propagation Equations

Pulse propagation in optical fibers is well describes by the Nonlinear Schrõdinger equations (NLSE) [1]. NLSE provides a canonical description for the envelope dynamics of quasi monochromatic plane wave propagating in a weekly nonlinear dispersive medium [77]. On short time and small propagation distance, the linear dynamics and cumulative nonlinear interactions result in a significant modulation of the wave amplitude on large spatial and temporal scales [30-31]. It expresses how the linear dispersion relation is affected by the thickening of the spectral lines associated to the modulation and resonant nonlinear interaction [1, 10]. In optics it can also be viewed as the extension to nonlinear media of the paraxial approximation, extensively used for linear beam propagating in random media [10].

5.2 Formulation of Propagation Equations: NLSE

The NLSE can be derived from the vector wave equation as

$$\nabla^2 \widetilde{\mathbf{E}} - k_0^2 \varepsilon_r \widetilde{\mathbf{E}} = 0 \tag{5.1}$$

The equation (5.1) can be solved by using method of separation of variable. Let's assume the solution is [1]

$$\widetilde{\mathbf{E}}(r, \omega - \omega_0) = F(x, y)\widetilde{A}(z, \omega - \omega_0) \exp(i\beta_0 z) \tag{5.2}$$

Here $\widetilde{A}(z, \omega)$ is the slowly varying function of distance z and β_0 is the wave vector at a center frequency, ω_0.

According to the separation of variable, equation (5.1) is separated into two equation with $F(x,y)$ and $A(z,\omega)$

$$\frac{\partial^2 F}{\partial x^2} + \frac{\partial^2 F}{\partial x^2} + [\varepsilon(\omega)k_0^{\;2} - \tilde{\beta}^2]F = 0 \tag{5.3}$$

$$2i\beta_0 \frac{\partial \tilde{A}}{\partial z} + (\tilde{\beta}^2 - \beta_0^{\;2})A = 0 \tag{5.4}$$

$\frac{\partial^2 \tilde{A}}{\partial z^2}$ is neglected in equation (5.4) because of the slowly varying approximation of A with z. $\tilde{\beta}$ is evaluated eigen value of the guided mode. In our case we evaluated this by using finite element method discussed in chapter 2. The dielectric constant $\varepsilon(\omega)$ can be approximated by

$$\varepsilon = (n + \Delta n)^2 = n^2 + 2n\Delta n \tag{5.5}$$

Here

$$\Delta n = n_2 |E|^2 \tag{5.6}$$

In first order perturbation theory, Δn does not affect the modal distribution $F(x,y)$. However the eigen value $\tilde{\beta}$ becomes

$$\tilde{\beta}(\omega) = \beta(\omega) + \Delta\beta \tag{5.7}$$

$$\Delta\beta = \frac{k_0 \iint \Delta n |F(x, y)|^2 \, dxdy}{\iint |F(x, y)|^2 \, dxdy} \tag{5.8}$$

Electric field for wave equation with first order perturbation can be written as

$$E(r,t) = \frac{1}{2} x\{F(x, y)A(z,t)\exp[i(\beta_0 z - \omega_0 t)] + c.c \tag{5.9}$$

Here $A(z,t)$ is the slowly varying pulse envelop whose Fourier transform is $\tilde{A}(z, \omega - \omega_0)$.

By approximating $(\tilde{\beta}^2 - \beta_0^2) = 2\beta_0(\tilde{\beta} - \beta_0)$ the equation (5.3) becomes

$$2i\beta_0 \frac{\partial \tilde{A}}{\partial z} + 2\beta_0(\tilde{\beta} - \beta_0)\tilde{A} = 0 \tag{5.10}$$

After some straight forward manipulation the above equation (5.10) becomes

$$\frac{\partial \tilde{A}}{\partial z} = i(\beta(\omega) + \Delta\beta - \beta_0)\tilde{A} \tag{5.11}$$

The equation (5.11) tells that each spectral component within the pulse envelope acquires a phase shift as it propagates. Replacing the $\beta(\omega)$ by its Taylor's series, equation (5.11) becomes

$$\frac{\partial \tilde{A}}{\partial z} = i((\omega - \omega_0)\beta_1 + \frac{1}{2}(\omega - \omega_0)^2\beta_2 + \frac{1}{6}(\omega - \omega_0)^3\beta_3 + \frac{1}{24}(\omega - \omega_0)^4\beta_4 + ... + \Delta\beta)\tilde{A} \tag{5.12}$$

Taking inverse Fourier transform which will replace $(\omega - \omega_0)$ by $i\dfrac{\partial}{\partial t}$ makes the equation (5.12)

as

$$\frac{\partial A}{\partial z} = -\beta_1 \frac{\partial A}{\partial t} - i\frac{1}{2}\beta_2 \frac{\partial A}{\partial t^2} + \frac{1}{6}\beta_3 \frac{\partial A}{\partial t^3} + i\frac{1}{24}\beta_4 \frac{\partial A}{\partial t^4} + ... + i\Delta\beta A \tag{5.13}$$

$\Delta\beta$ represents the nonlinearity and can be evaluated by equation (5.6) and (5.8). Replacing $\Delta\beta$ in equation (5.13) results

$$\frac{\partial A}{\partial z} = -\beta_1 \frac{\partial A}{\partial t} - i\frac{1}{2}\beta_2 \frac{\partial A}{\partial t^2} + \frac{1}{6}\beta_3 \frac{\partial A}{\partial t^3} + i\frac{1}{24}\beta_4 \frac{\partial A}{\partial t^4} + ... + i\gamma|A|^2 A \tag{5.14}$$

γ is the nonlinear cross-coupling parameter and can be expressed as

$$\gamma = (\frac{n_2\omega_0}{cA_{eff}}) \tag{5.15}$$

50

Here c is the speed of light, and Effective area, A_{eff} was evaluated analytically by using the following expression involving electric field E(x,y) of the evaluated from the finite element solution.[55]

$$A_{eff} = \frac{(\iint |E(x,y)|^2 dxdy)^2}{\iint |E(x,y)|^4 dxdy}$$
(5. 16)

Even though the NLSE does not provide a complete physical description of a system, it is the basis for modeling optical-fiber communication systems [1]. Indeed, one can modify the NLSE to incorporate various effects such as fiber loss, third-order dispersion, amplification, multi photon absorption, scattering and amplified spontaneous noise to obtain a more realistic model of optical fiber transmissions [73, 78]. In the case of anomalous dispersion, the NLSE has well-known analytical soliton solutions that give deep physical insight into the nature of self-phase modulation and dispersion [73, 79]. However, in almost all realistic cases, inclusion of higher-order effects and scattering makes the propagation equation not analytically solvable. A numerical approach is then necessary. The most commonly used numerical scheme to solve the NLSE is the Split-Step Fourier Method (SSFM), which is convenient for its simplicity and flexibility in dealing with higher-order effects [73].

5.3   Coupled Mode Equation for Coupled Structure

When two identical fibers are brought close together, coupling of the evanescent field between the weakly guiding fibers are observed. This interaction gives a coupling parameter. If the Kerr nonlinearity is included the traditional model consists of two coupled nonlinear Schrödinger equations stated in equation (5.17) as [79]

51

$$\frac{\partial A_1}{\partial z} = -\beta_1 \frac{\partial A_1}{\partial t} - i\frac{1}{2}\beta_2 \frac{\partial A_1}{\partial t^2} + \frac{1}{6}\beta_3 \frac{\partial A_1}{\partial t^3} + i\frac{1}{24}\beta_4 \frac{\partial A_1}{\partial t^4} + ... + i\gamma|A_1|^2 A_1 + \kappa_{12}A_2 \qquad (5.17a)$$

$$\frac{\partial A_2}{\partial z} = -\beta_1 \frac{\partial A_2}{\partial t} - i\frac{1}{2}\beta_2 \frac{\partial A_2}{\partial t^2} + \frac{1}{6}\beta_3 \frac{\partial A_2}{\partial t^3} + i\frac{1}{24}\beta_4 \frac{\partial A_2}{\partial t^4} + ... + i\gamma|A_2|^2 A_2 + \kappa_{21}A_1 \qquad (5.17b)$$

where A_1 and A_2 refers to the envelope of the electromagnetic wave in waveguides 1 and 2, respectively, κ_{mn} is the normalized linear cross coupling constant expressed as

$$\kappa_{mn} = \frac{\omega}{4P_n} \iint (\varepsilon' - \varepsilon)e_m e_n dxdy \qquad (5.18)$$

ε' is permittivity after perturbation, $\vec{e}$ is the electric field and P_n is the normalized power in each waveguide and can be expressed as

$$P_n = \frac{1}{2} \iint \vec{e}_n . \vec{h}^*_n dxdy \qquad (5.19)$$

$\vec{h}$ is the magnetic field. For two identical waveguide the $\kappa_{21=}\kappa_{12=}\kappa$.

The linear coupling is due to evanescent field coupling and the nonlinear coupling is due to cross-phase modulation. In dual core nonlinear fiber couplers, the overlap between the two modes corresponding to each core is small and the cross-phase-induced coupling is usually neglected [59]. In a linear coupler the power exchanged between two wave guides follows a sinusoidal pattern [59]. Previous study for regular optical fiber coupler in [7, 59] shows that the switching occurs for the power of 4κ. Later in this chapter we will compare this with our results for the PCF coupler. For linear continuous wave it is common in the literature to define two lengths [1, 59]. One is the distance at which the initial power incident on one of the waveguide returns fully to the original waveguide called full-beat length. Another one is half of this distance known as half-beat length. It is also referred to as the coupling length Lc [59].

5.4   Ultra Short Pulses

By saying ultra short we mean pulse in femto second (10^{-15}s) range. This time scale becomes accessible because of the progress in the generation, amplification and measurements of ultra short pulse [80]. Due to large energy concentration this topics encompasses the study of interaction of intense laser with mater, as well as transient response of atoms and molecules and basic properties of the fs radiation itself [80-82]. Right after the invention of laser in 1960s scientific communities were working on producing short light pulses in laser. In 70's progress in laser physics open the door of pico-second pulse generation which was continued in 80's to achieve femto second pulse [80].

Femto second technology opens up new fascinating possibilities based on some unique properties of ultra short light pulses which include [80-82]:

- Energy can be concentrated in a temporal interval as short as fs which corresponds to a few optical cycles in the visible range.

- Pulse peak power can be extremely large even at moderate pulse energies. e.g. for 100 fs pulses an energy of 1 nJ exhibits an average power of 10 MW. Focusing this pulse to a 100 μm^2 spot will generate an intensity of 20 TW/cm^2

- Geometrical length of a femto second pulse amounts only to several μm. Such a coherence length is usually associated with incoherent light. The essential difference is that incoherent light is generally spread over a much longer distance.

Faster data transfer and processing is possible by utilizing this faster carrier frequency and subsequent higher bandwidths. A variety of reversible as well as irreversible nonlinear processes become accessible due to the large intensities of fs pulses. There are proposals to use

53

such pulses for laser fusion [87]. Because of large energy concentration in a very short duration it is possible to utilize nonlinear processes in fiber and other optical-electronic devices.

5.4.1 Ultra Short Pulse Propagation through PCF Coupler

It requires anomalous dispersion to support undistorted propagation of short pulses [1]. As from our previous dispersion analysis we have seen that the PCF demonstrate anomalous dispersion in both 1.31 μm and 1.55 μm windows. Pulse propagation through this coupled structure has been described by the following equations (5.20). This equation was numerically solved using beam propagation method [14].

$$i\frac{\partial q_1}{\partial z} - \frac{\beta_2}{2}\frac{\partial^2 q_1}{\partial \tau^2} - i\frac{\beta_3}{6}\frac{\partial^3 q_1}{\partial \tau^3} + \gamma(|q_1|^2 + c_x|q_2|^2)q_1 + \kappa_0 q_2 + \kappa_1\frac{\partial q_2}{\partial \tau} = 0 \quad \text{(5.20 a)}$$

$$i\frac{\partial q_2}{\partial z} - \frac{\beta_2}{2}\frac{\partial^2 q_2}{\partial \tau^2} - i\frac{\beta_3}{6}\frac{\partial^3 q_2}{\partial \tau^3} + \gamma(|q_2|^2 + c_x|q_1|^2)q_2 + \kappa_0 q_1 + \kappa_1\frac{\partial q_1}{\partial \tau} = 0 \quad \text{(5.20b)}$$

z and τ are the operator of the derivatives, in this case are distance and time respectively. Here q refers to the envelope of the electromagnetic wave; C_x is the parameter for cross phase modulation (XPM)

$$C_x = 2n_2 k_0 \iint |E_1(x,y)|^2 |E_2(x,y)|^2 dxdy \quad \text{(5.21)}$$

A_{eff} of the dual core PCF is shown with wavelength in Figure 5.1. A noticeable increment is observed as the wavelength increases. We picked up the values at 1.55 μm and 1.31 μm for the evaluation of γ at those wavelengths.
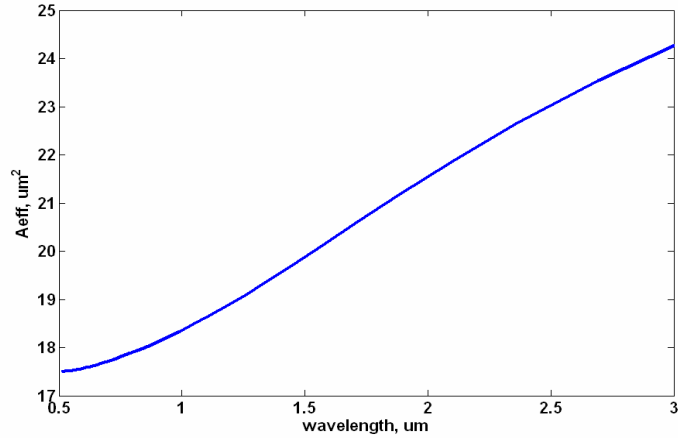
Figure 5.1 Effective core area of PCF couplers (d=1.0 µm, C=5µm and d/Λ =0.4).

Figure 5.2 shows the femto second pulse propagated though the PCF couplers. It is observed that the energy is transferred from the bar channel (the waveguide which received the input pulses) to the other waveguide named as cross channel after traveling *Lc* (in this case is 21 mm). The result shows similar coupling characteristic as that of the nonlinear optical fiber directional coupler made of two optical fibers reported in ref [79]. The specialties of these PCF couplers are: they are relatively short and coupling and dispersion can be altered by designing the core and cladding geometry which we already have demonstrated in the previous chapters.
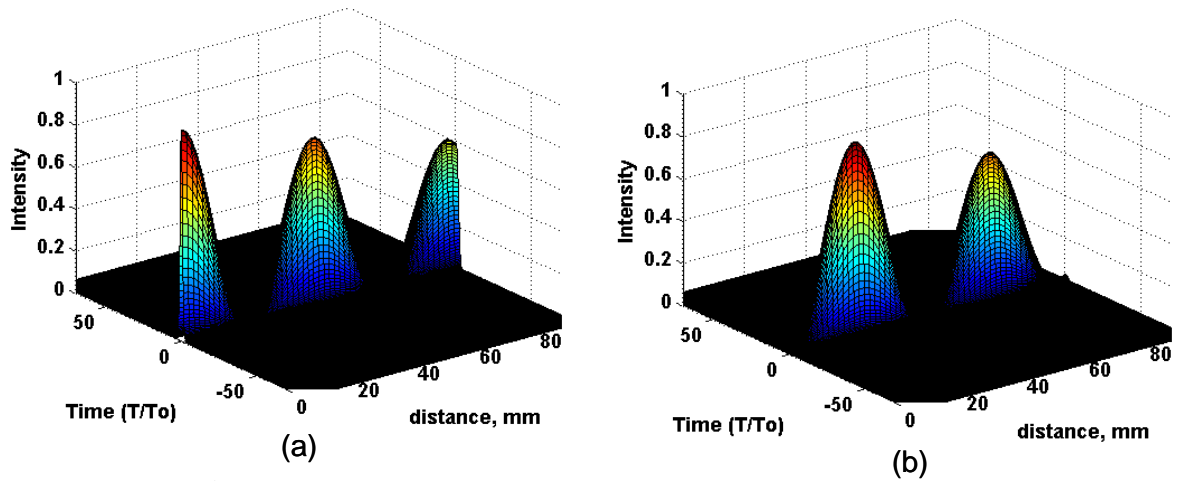
Figure 5.2 1550 nm pulse propagation through the PCF coupler
(d=1.0 μm, C=5 μm and d/Λ =0.4) (a) bar channel and (b) cross channel

Figure 5.3 shows the power propagation through the bar channel (waveguide with input pulse) of the coupler at the above two wavelengths. It is observed that the coupling length at 1.55 μm is shorter than that of at 1.31 μm.
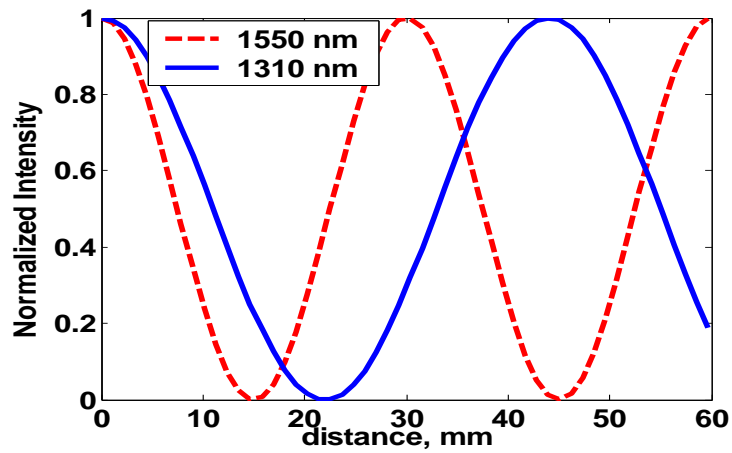

Figure 5.3 Normalized power in bar channel of PCF couplers (d=1.0 μm, C=5μm and d/Λ =0.4)

5.4.2   Dispersion Effects on the Pulse Propagation

When a pulse propagates a substantial distance then it experiences dispersion. Group velocity dispersion β_2 causes the pulse broadening and β_3 is responsible for oscillation in the rising or the trailing edge depending on its sign [1]. Figure 5.4 shows the input and output pulse shapes at 1.55 and 1.31 μm wavelengths for a 21 cm (around 10 times of the coupling length) PCF coupler.
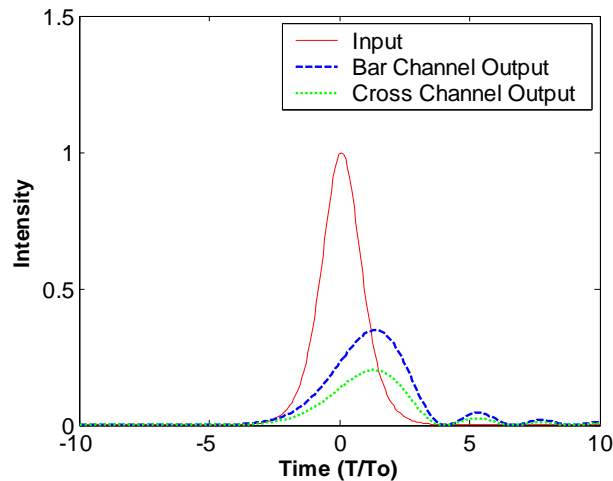

Figure 5.4 Input and output pulse of the PCF cores of PCF coupler
(d=1.0 μm, C=5 μm and d/Λ =0.4) at 21cm for 1.55um
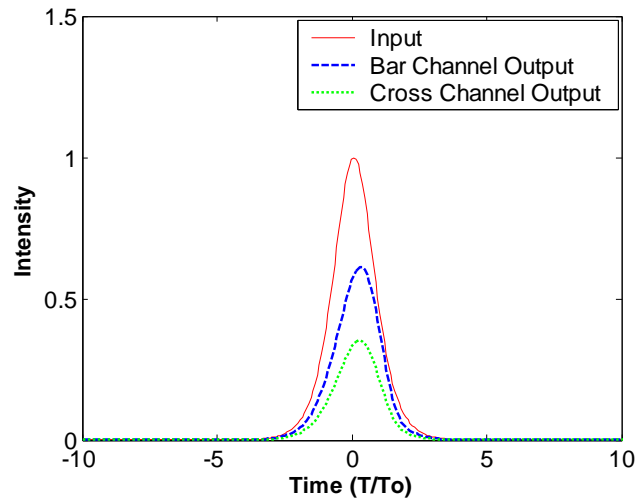
Figure 5.5 Input and output pulse of the PCF cores of PCF coupler
(d=1.0 μm, C=5 μm and d/Λ =0.4) at 21cm for 1.31um

It is observed from the bar and cross channel output pulses that, at 1.55 µm the pulse undergoes compression effect in the rising edge and in the trailing edge it expand due to positive β_3. Also positive β_3 causes oscillation at the trailing edge of the pulse. On the other hand at 1.31 µm (Fig. 5.5) this dispersion and the above mentioned oscillation effects are not observed as both β_2 and β_3 are close to zero.

Pulse spreading due to the dispersion can be carefully controlled by increasing the power. Fig. 5.6 shows the input and output of 1.55 µm pulses at 6 cm for 1W and 10 W of peak power respectively. For 1W power the pulse demonstrates spreading due to β_2. This was compensated by increasing the power to 10 W that preserve the integrity of the pulse.

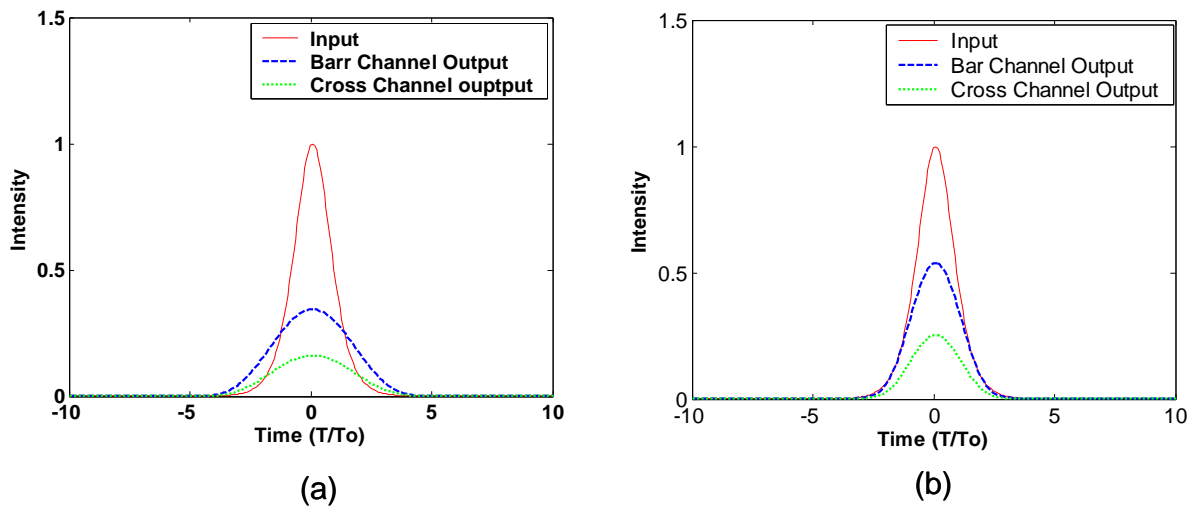(a)   (b)

Figure 5.6 Input and output pulse of the PCF cores at 6cm for (a) 1W and (b) 10 W

5.4.3 Third Order Dispersion on Soliton Pulse

Even though the contribution of β_2 is the most dominant in major practical applications but still it is necessary to include the third order term proportional to β_3. For example around zero dispersion wavelength region β_3 contribute most to the GVD effect [1]. For ultra short pulses ($\tau_0<1ps$) β_3 is a necessary parameter to be included. Changing sign of β_3 shows the change of symmetry of the pulse shape. For soliton pulse flowing through fiber with positive value causes oscillation at the trailing edge of the pulse. On the other hand for negative β_3 oscillation appeared at the rising edge of the pulse [1]. Fig 5.7 and 5.8 shows the effect of β_3 on the soliton pulse.
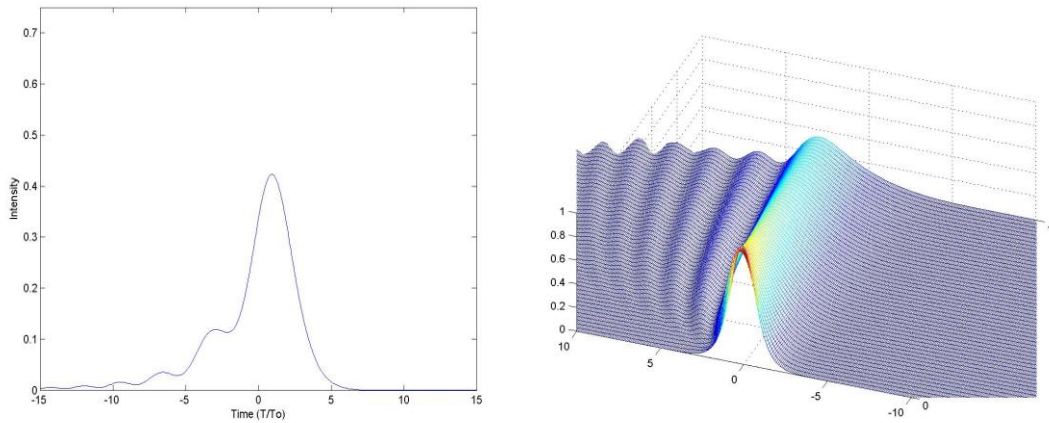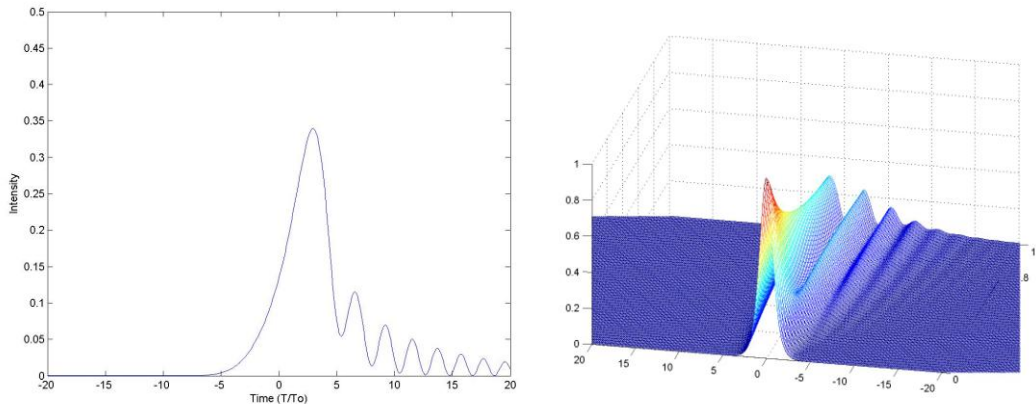
Figure 5.7 2D and 3D pulse shape for negative β_3

Figure 5.8 2D and 3D pulse shape for positive β_3

For the PCF coupler discussed above (d=1.0 μm, C=5μm and d/Λ =0.4), both the dispersion and coupling length at 1310 nm are less than those at 1550 nm. From our model we found that the Lc at 1310 nm is 21 mm, β_2 is -4 ps^2/km and β_3 is 0.075 ps^3/km and those values at 1550 nm are 19 mm, -24 ps^2/km and 0.115 ps^3/km respectively. For a 38 mm long device, less than (~1nJ) pulse energy was required to distort the pulse at 1310 nm. This value is 6nJ at 1550 nm. The primary reason is that the PCF has less β_2 and β_3 at 1310 nm than at 1550 nm.

Also as shown in Figure 5.9, a 2 nJ pulse with 100 fs duration had a tilted trailing edge at 1310 nm, whereas at 1550 nm the pulse shape remain undistorted. At 1310 nm, β_2 is small since it is close to λ_d , but β_3 is still large. On the other hand, at 1550 nm β_2 is comparably higher than that at 1310 nm. That is why β_3 effect looks more prominent at 1310 nm.
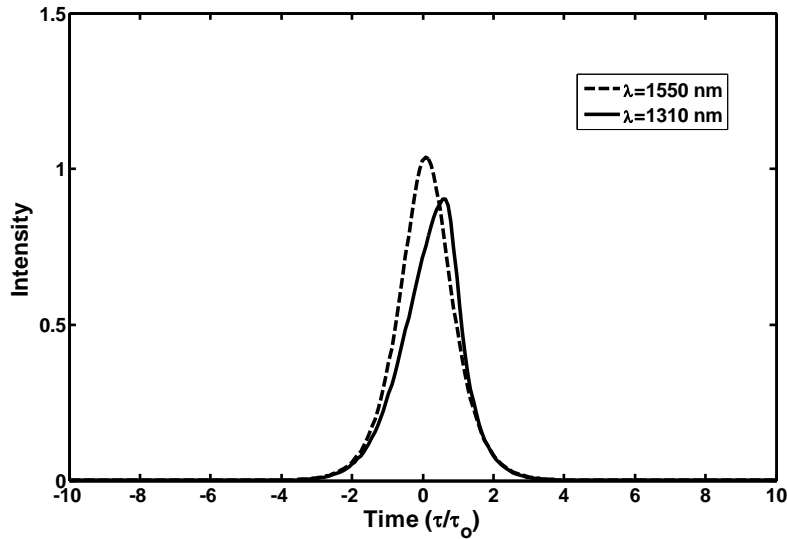

Figure 5.9 100 fs pulse at the bar channel output of 38 mm PCF coupler
(d=1 μm, C=4Λ and d/Λ =0.4)

CHAPTER 6:   SWITCHING IN NONLINEAR DUAL CORE PCF

6.1   Introduction to All Optical Switch

For the last few years demand for high bandwidth in telecommunication is increasing rapidly. High growth rate of Internet Protocol (IP) traffic is the primary cause of this bandwidth increase. Moreover real time video application is forcing the carrier to extend their existing optical network even to household [60, 83]. With their improved efficiency and lower costs, optical switches provide the carriers to manage the new and competitive dense wavelength division multiplexing (DWDM) networks. Wave-guide switches were among the first all-optical switches to be developed. Fiber optic cable, semiconductor laser cavities and PCF are other examples of wave guides. If two optical waveguides are coupled together then we can use a control stimulus to change the refractive index from one part of the waveguide to other. The interference effect at waveguide 1 is now changed, which causes the light being switched to output of wave-guide 2. In brief optical power is exchanged between the coupled cores due to weak overlap of adjacent electric field. Coupled optical waveguide shows potential of being used as all optical switch. In recent year's considerable research work has been conducted on twin core fiber used as a nonlinear coupler for switching application [59, 73, 79]. Nonlinear directional coupler (NLDC) made of two optical fiber is a well known all optical switch [86]. NLDC can be implemented in dual core PCF [21, 53, 84]. These devices can be relatively short which bring the prospect of having compact switch configuration [21, 53-55]. Experiment shows that all optical switching occurred in these types of couplers [21]. Theoretical treatment of femto second pulse switching in dual core PCF has been presented in this chapter to explain the

switching action in the experiment done in ref [21]. In order to support soliton switching we also adjust the PCF coupling and dispersion parameters by changing the PCF geometry used in our finite element calculation.

6.2   Nonlinear Directional Coupler (NLDC)

NLDC is usually made by placing two cores in a close proximity so the electric field can be coupled from one core to the other. The nonlinear coupled optical waveguide functions in the following manners: for low input power the beam is transferred from one wave guide to the other, but for high input power the beam remains in the same wave guide (Fig. 6.1) [21,79]. It was demonstrated numerically that if the input pulse is soliton then the pulse in the two core of twin core fiber came out with minimum or almost no distortion [55, 85]. Similar like in twin core fiber, switching can also be achieved in the dual core PCF. Soliton solution of coupled nonlinear Schrõdinger equations (CNLSE) is used to determine that. The necessary parameters of CNLSE are derived from our FEM. Design effort has been made to adjust these parameters to achieve the desired intensity dependent switching action.
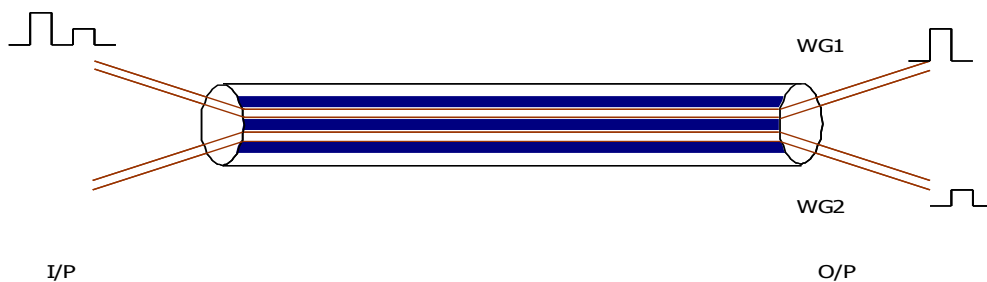

Figure 6.1 Couple twin core fiber

6.3   Soliton Pulse Propagation through Designed PCF Coupler

Depending on the excitation wavelength, the couplers implemented in dual core PCFs are capable of supporting soliton pulses noting that anomalous dispersion is required to support soliton pulses for the self-focusing nonlinearity of silica glass. The dual core PCFs considered here support soliton in both the 1.31 μm and 1.55 μm telecommunications windows as both of this two wavelength experiences anomalous dispersion [1, 55].

For our designed PCF coupler with (d=2.0 μm, C=2Λ and d/Λ =0.9), A_{eff} was evaluated as 41 μm^2 at 1.55 μm. Value of Lc differs significantly by altering the PCF geometry [53-54]. We increase the coupling length by increasing the d/Λ which we reported in ref [55]. L_C for the above mentioned PCF is evaluated as 1.8 cm at 1.55 μm. Our FEM model provides us the wave vector k_z. From that we evaluate the group velocity dispersion β_2 at 1.55 μm as -47ps^2/km. Subsequently third order dispersion β_3, is also been evaluated as 0.1 ps^3/km.

Fig. 6.2 shows that a soliton pulse is propagating through the PCF coupler. The energy is transferred from the bar channel (the waveguide which received the input pulses) to the other waveguide (named the cross channel) after traveling L_C which is 1.8 cm. For a 100 fs pulse propagating through this waveguide at 1.55 um wavelength the soliton period $Z_0=1.57(T_0^2/\beta_2)$ =33 cm [1, 55]. Note that there is no pulse break-up in the time domain, at least until Z_0. From our calculation at least 80 nJ is required for soliton pulse to propagate [86]. The result shows similar coupling characteristic as that of the nonlinear optical fiber directional coupler reported in ref [79].
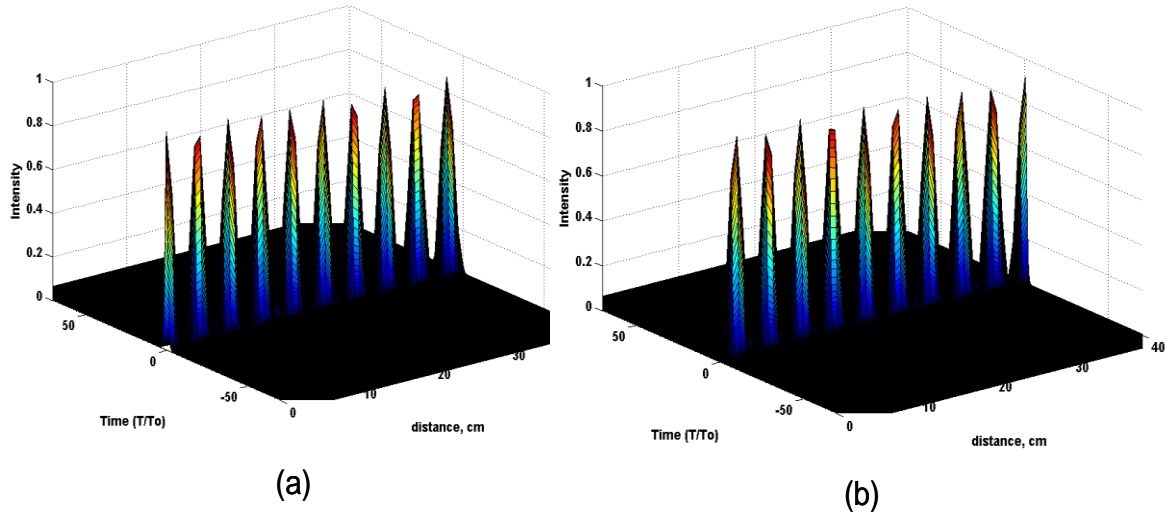
Figure 6.2. Soliton pulse propagation at 1.55 μm through the PCF coupler with d=2.0 μm, and d/Λ =0.9 (a) bar channel and (b) cross channel

Similarly the 2D view of 100 fs pulse depicts the soliton pulse propagation. At lower peak pulse power (at 20W) the pulse experiences only dispersion and causes pulse broadening shown in Fig 6.3(a). When we increase the peak power (around 800W) the nonlinearity starts taking over and cancel out the dispersion. Fig. 6.3(b) shows the undistorted soliton pulse.
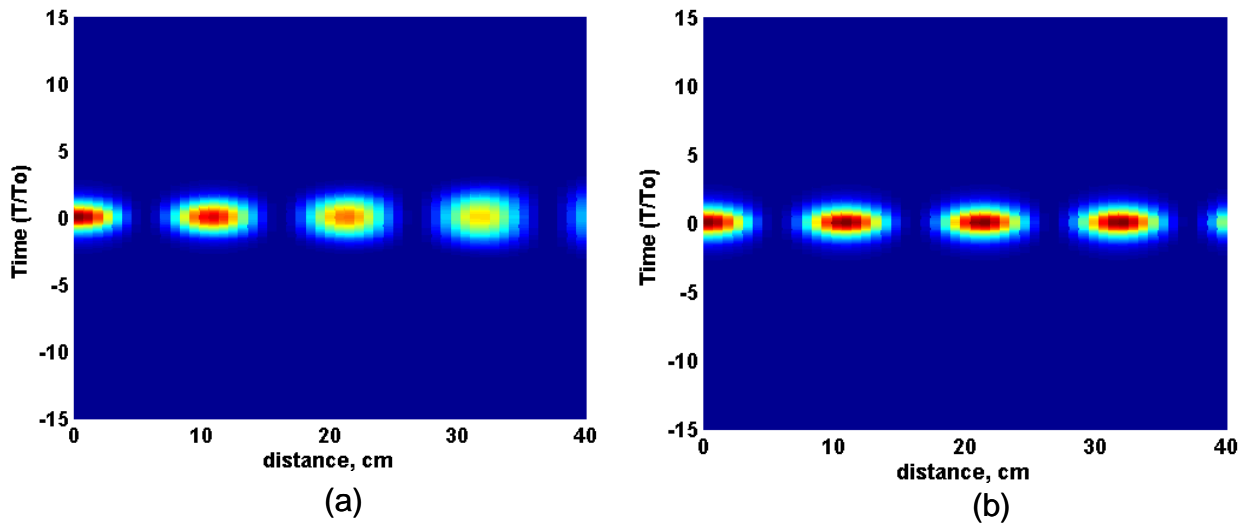

Figure 6.3 2D view of 100 fs pulse propagation through the bar channel of PCF in Fig. 1 (a) Dispersed pulse at 20W peak power (b) Soliton pulse at 800W peak power

6.4 Pulse Switching in Dual Core PCF

At low peak intensity of the pulse, the dual core PCF behaves like a linear coupler. The two core completely exchange power after traveling a distance of *Lc*. As the intensity increases the power remain in the same waveguide where the pulse was originally launched. Figure 6.4 shows this clearly. Here we see that at low intensity the normalized power P_1 in bar channel (the PCF core which receive the input pulse) and P_2 in the cross channel (another PCF core) completely exchanged after propagating 1.8 cm which is the coupling length of our PCF. This linear characteristic is shown in Figure 6.4 (a). On the contrary at higher intensity shown in Figure 6.4 (b) the power tends to remain in the same core. Transmission curve at Figure 6.5 elaborate the switching characteristic prominently. We observe switching around 1.6 TW/cm^2.

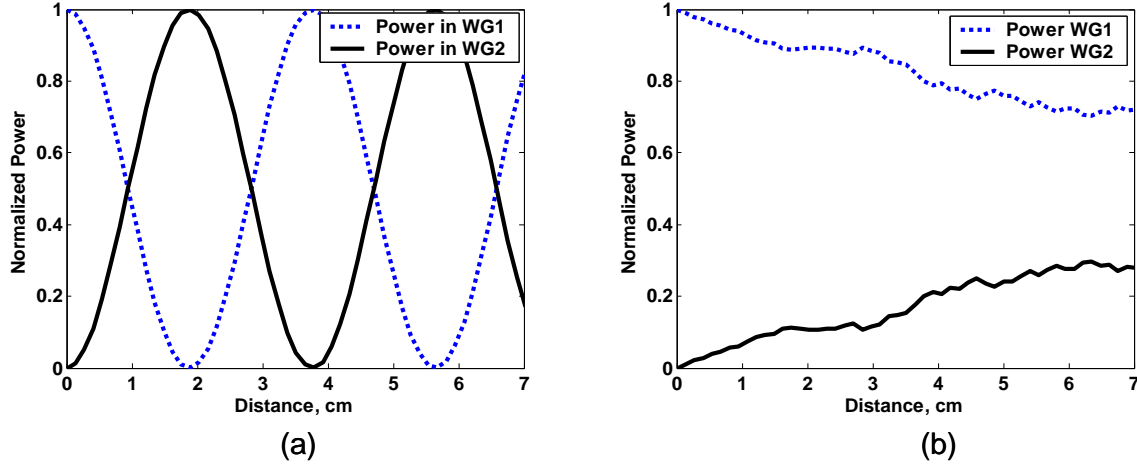(a)   (b)

Figure 6.4 Normalized power in bar channel P_1 and cross channel P_2
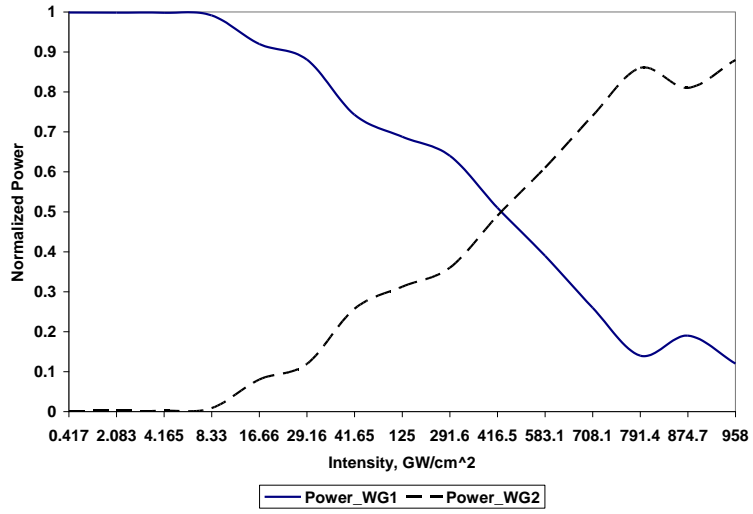(a) at 4.16 GW/ cm^2 (b) at 583 GW/ cm^2

Figure 6.5 Transmission curve of dual core PCF (d=2.0 µm, C=2Λ and d/Λ=0.9) versus input intensity

CHAPTER 7:   CONTINUUM GENERATION IN PCF

7.1   Introduction: Continuum Generation by Ultra Short Pulse

One of the most impressive and simple experiments with ultra short light pulses is the generation of a white light continuum [49]. At the same time continuum generation with laser pulses is one of the most complex and difficult to analyze processes as it combines special and temporal effects and their interplay [49, 52, 86]. Focusing a powerful laser pulse into a transparent material results substantial spectral broadening [22, 86]. The output pulse appears on a sheet of paper as a white light flash, even if the exciting pulse is in the near infrared (IR) or near ultraviolet (UV) spectral range. This is often accompanied by colors distributed in rings. Continuum generation was first discovered with pico second pulses by Alfano and Shapiro [94] and has since been applied to numerous experiments [86-88]. One of the most attractive applications is time-resolved spectroscopy, where the continuum pulse is used as a ultra fast spectral probe.

Spectral supper broadening was observed in many different materials including liquids, solids, and gases. Essential processes contributing to the continuum generation are common to all. Supper continuum does not have a flat uniform spectrum [88-89]. The dominant process and the starting mechanism leading to spectral supper broadening is the SPM, because of an intensity-dependent refractive index. However, a number of other nonlinear effects play a role as well. The various nonlinear processes make the exact treatment of the continuum generation with short pulses, extremely complex. FWM and SRS are also needed to be considered. The strong anti stocks component visible in the experiment is likely because of multi photon excitation of

the dielectric material followed by avalanche ionization [88-90]. The resulting electron plasma in the conduction band produces a fast rise of a negative refractive index component that can explain the dominant broadening toward the shorter wavelengths [89]. SPM associated with self focusing leading to extremely high intensities where the beam collapses. It is at this point where the continuum generating nonlinear processes is most effective [89].

Traditionally continua were generated in bulk materials with amplified femto second pulses [89-92]. Pulse continues to broaden due to dispersion until beam collapse limited the effective material length. This situation changed with the introduction of microstructured fibers [87-91]. These fibers either shift the zero dispersion wavelengths to regions were fs oscillator pulses were readily available and/or reduce the dispersion while increasing the nonlinearity [21, 55]. Because of   the possible large propagation lengths for guided modes the overall nonlinear interaction length can be greatly increased, which allowed the generation of continua with nJ and sub-nJ pulses directly from oscillators, and even using continuous wave (CW) light [59]. Using pulses directly from Ti: sapphire oscillators, continua covering almost two decades from 370 nm to 1600 nm [89].

7.2   The Physics of Super Continuum Generation

The physical processes behind suppercontinum generation in fibers can be very different, depending particularly on the chromatic dispersion and length of the fiber, the pulse duration, the initial peak power and the pump wavelength. When femtosecond pulses are used, the spectral broadening can be dominantly caused by self-phase modulation. In the anomalous dispersion regime, the combination of self-phase modulation and dispersion can lead to complicated soliton

dynamics, including the split-up of higher-order solitons into multiple fundamental solitons (soliton fission) [19,87]. For pumping with pico second or nanosecond pulses, Raman scattering and four-wave mixing can be rather important [89].

In some cases, such as with self-phase modulation being the dominant mechanism and the dispersion being normal, the process is very deterministic, and the phase coherence of the generated suppercontinum pulses can be very high, even under conditions of strong spectral broadening. In other cases (e.g. involving higher-order soliton effects), the process can be extremely sensitive to the slightest fluctuations (including quantum noise) e.g. in the input pulses, so that the properties of the spectrally broadened pulses vary quite substantially from pulse to pulse [89]. The strongly nonlinear nature of suppercontinum generation makes it hard to intuitively understand all the details of the interaction, or to predict relations with analytical tools. Therefore, numerical pulse propagation modeling (often with special precautions due to the extreme optical bandwidth) is required for the analysis of such processes. Intuitive pictures or analytical guidelines can be tested by comparison with results from such numerical models.

7.3   Experimental Demonstration of Multi Frequency Generation in PCF Coupler

Recently one research group experimentally demonstrated the multi frequency generation below 1550 nm for dual core PCF [21]. The observations in ref [21] reveal that the most of the input radiation has been converted to other frequencies. At lower intensities the power spectrum is broadened by self-phase modulation. On the other hand for higher intensity spectral broadening still continues below 1500 nm. Two peaks observed at 600 nm and 1800 nm and their conclusion is due to third harmonic generation.

7.3.1   Explanation of Multi Frequency Generation using the Developed Models

Highly nonlinear PCF has the capacity to generate higher frequencies due to multiple nonlinear process such as SPM, Raman Scattering, four wave mixing (FWM). Experimental results for dual core PCF geometry confirm this [21]. Theoretically explaining the results required numerical treatment of PCF to infer necessary dispersion, nonlinear and coupling parameters for a wide frequency spectrum. Our FEM did that successfully and then we use these fitting parameters in the CNLSE for the pulse propagation treatment.

At higher input power, it is evident that the other frequencies generate due to several nonlinear processes. It was quickly realized from the experiment that the switching characteristics deteriorated due to energy transfer from one frequency to another [21]. Multiple nonlinear processes such as SPM, SRS and wave-mixing were responsible for the high frequency generation. As the frequency covers a broad spectrum, so it was essential to incorporate wide spectrum of dispersion and coupling characteristic in our model. We include all these and modify the propagation equation as

$$i\frac{\partial q_1}{\partial z} - \frac{\beta_2}{2}\frac{\partial^2 q_1}{\partial \tau^2} - i\frac{\beta_3}{6}\frac{\partial^3 q_1}{\partial \tau^3} + \frac{\beta_4}{24}\frac{\partial^4 q_1}{\partial \tau^4} + \gamma(|q_1|^2 + \eta|q_2|^2)q_1 +$$
$$i\frac{\gamma}{\omega}\frac{\partial}{\partial \tau}(q_1|q_1|^2) - \gamma q_1 T_R \frac{\partial}{\partial \tau}(|q_1|^2) + \kappa_0 q_2 + \kappa_1 \frac{\partial q_2}{\partial \tau} = 0 \tag{7.1a}$$

$$i\frac{\partial q_2}{\partial z} - \frac{\beta_2}{2}\frac{\partial^2 q_2}{\partial \tau^2} - i\frac{\beta_3}{6}\frac{\partial^3 q_2}{\partial \tau^3} + \frac{\beta_4}{24}\frac{\partial^4 q_2}{\partial \tau^4} + \gamma(|q_1|^2 + \eta|q_2|^2)q_2 +$$
$$i\frac{\gamma}{\omega}\frac{\partial}{\partial \tau}(q_2|q_2|^2) - \gamma q_2 T_R \frac{\partial}{\partial \tau}(|q_2|^2) + \kappa_0 q_1 + \kappa_1 \frac{\partial q_1}{\partial \tau} = 0 \tag{7.1b}$$

β_4 shown in the fourth term is the fourth derivative of the wave vector k_z with respect to ω. T_R is the nonlinear response function originated from delayed Raman response. Experimentally T_R was

measured as 3 fs at 1.55 μm [1]. κ_0 is the coupling coefficient, which is related to the even and odd mode wave vector by

$$\kappa_0 = \frac{k_{ze} - k_{zo}}{2} = \frac{\pi}{2L_c} \tag{7.2}$$

κ_1 is the first derivative of κ_0 with respect to ω. This κ_1 term is added in the propagation equation to incorporate the frequency response of the coupling. Frequency dependent dispersion and coupling characteristics of PCF specimen used in the experiment was evaluated using FEM model and those agree well with the experimental results. Experimentally Lc can be measured by using cut back method and at 1.55 μm it was measured as about 5.6 mm for the PCF coupler used in [21]. Evaluated Lc from our model confirms this result (Figure 7.1). Figure 7.2 shows the frequency response of κ_0 and κ_1.
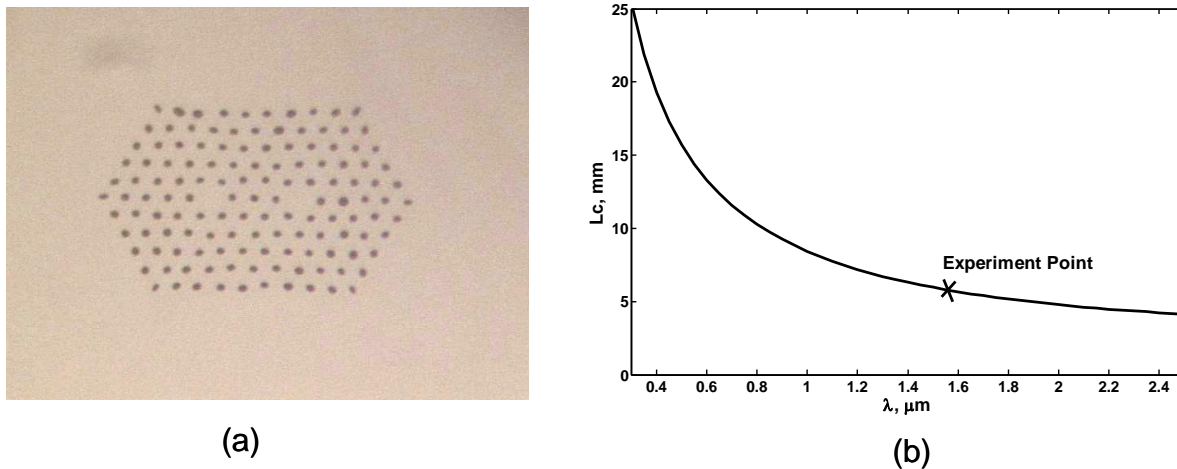

(a)

(b)

Figure 7.1 Coupling length of the dual core PCF sample (Five rings, d=1.0 μm, Λ =2.5μm and C=10 μm): (a) PCF geometry (b) *Lc*

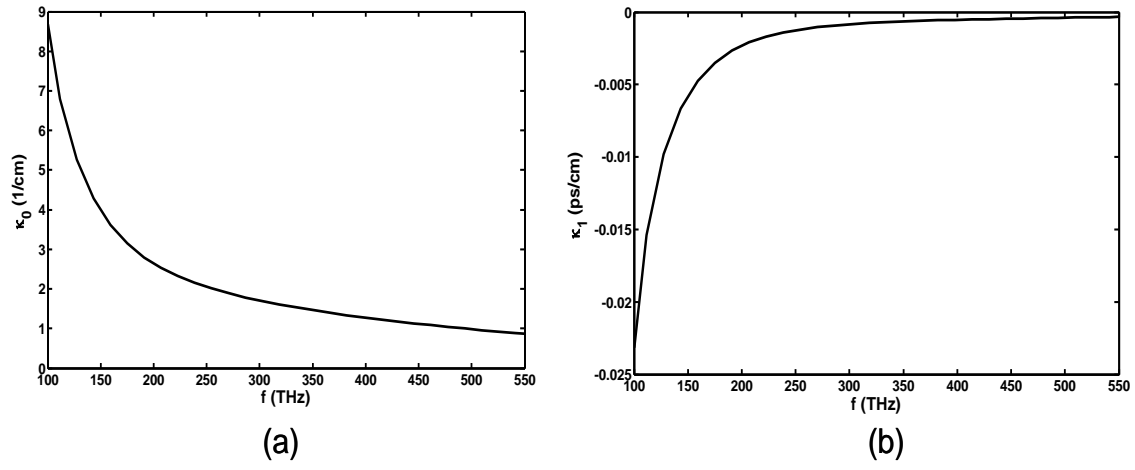**Figure 7.2** Coupling coefficient of the dual core PCF sample: (a) κ_0 (b) κ_1
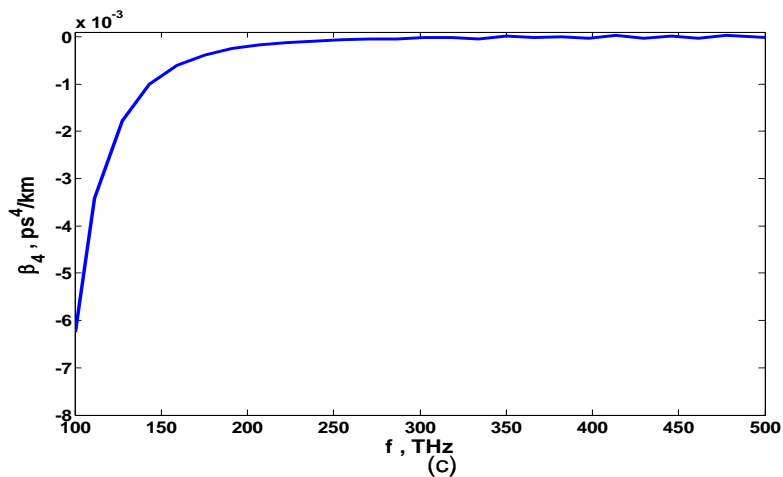
Figure 7.3 shows the frequency response of β_2, β_3 and β_4 of the dual core PCF sample used in the experiment. From our evaluated dispersion results it is found that the GVD shift from normal to anomalous region in around 1.1 μm (equivalent to 2.72 THz) which is also known as the zero dispersion wavelength λ_d and can be shifted by changing the d/Λ [55].
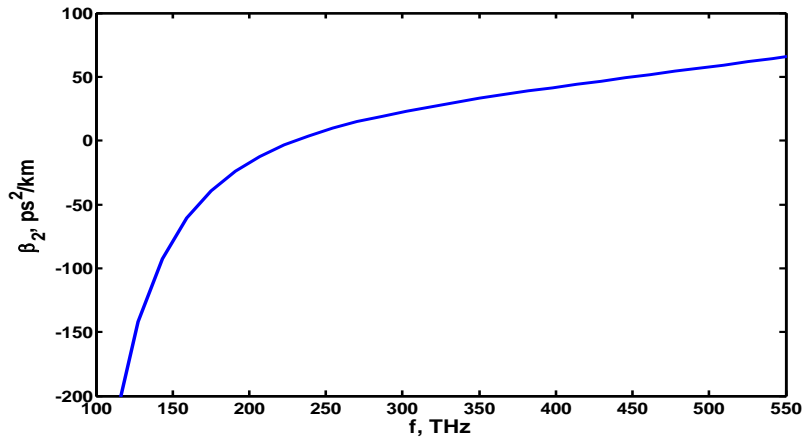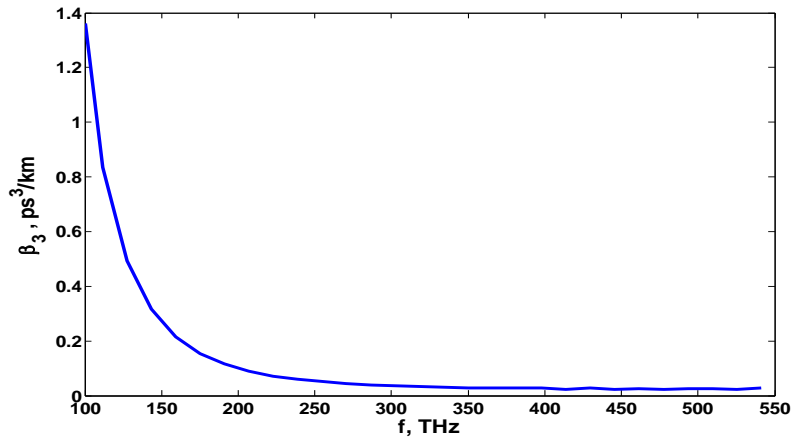
Figure 7.3 Frequency dependent dispersion characteristics of the PCF sample (a) β_2 (b) β_3 and (c) β_4

As the input peak pulse power increases beyond the switching threshold power, we observed breaking up of pulse primarily due to intense effect of SPM. Figure 7.4 shows the intensity of output pulses (both at bar and cross channel) for peak power of 10, 50, 75 and 114 KW respectively. At a relatively lower input power (up to 10 KW), distortion free pulse propagation is observed. Pulse could not keep its shape as the power increased. As we observe from the figures that the intensity modulation is more intense as the power increased. It is obvious from the time domain response shown in Figure 7.4 that higher input power causes higher frequency generation due to multiple nonlinear processes which was later confirmed by the frequency domain analysis. Fig 7.5 shows the wavelength response of cross channel output for a 1.55 μm input pulse at a power level of 10, 50, 75 and 114 KW respectively. We observe new frequency generation due to increased peak power. Pulse energy spread into a wide wavelength range (from 0.5 μm to 3.0 μm). Primary reason for this higher frequency generation is due to SPM. A 0.12 um higher wavelength shifting is observed due to SRS. Fig. 7.6 and 7.7 shows the 3D view of frequency response of both bar and cross channel respectively. The figures show that the higher frequency generated at the far end of the waveguide. Close to the input side, the pulse maintains its shape but as distance increases pulse starts introducing higher frequencies at higher input power.
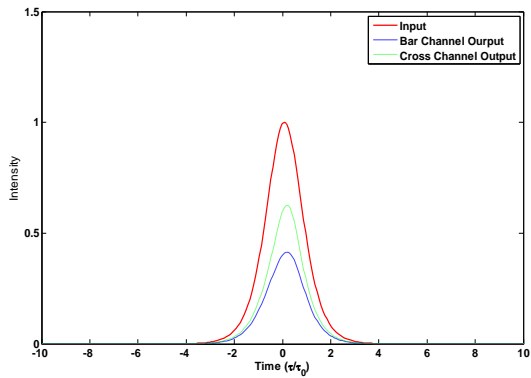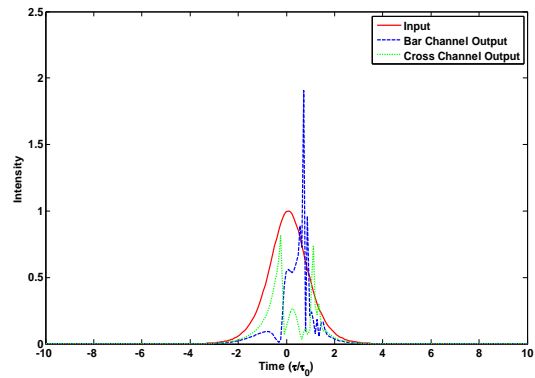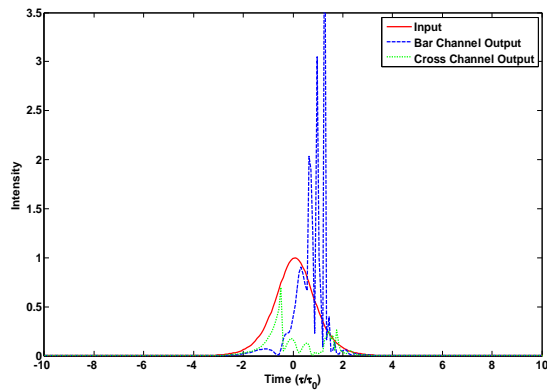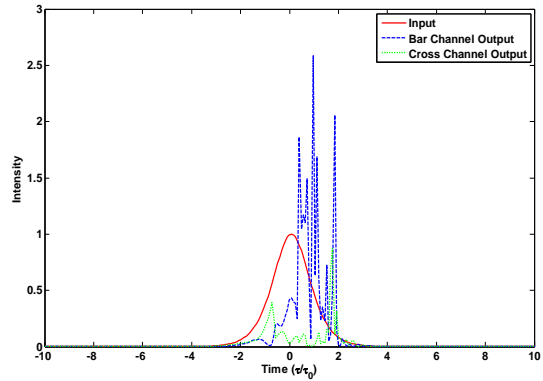
Figure 7.4 Input and output (both bar and cross channel) pulse shape of 9mm PCF sample
(a) at a peak pulse power of: (a) 10KW (b) 50 KW (c) 75 KW and (d) 100 KW
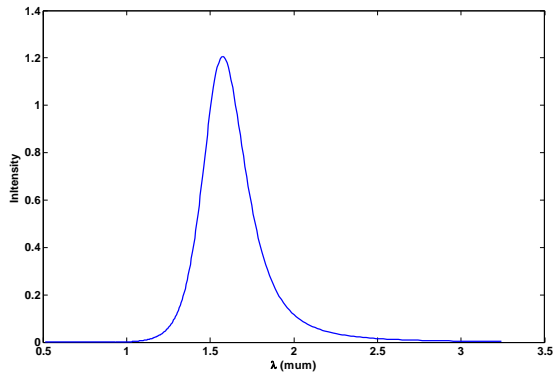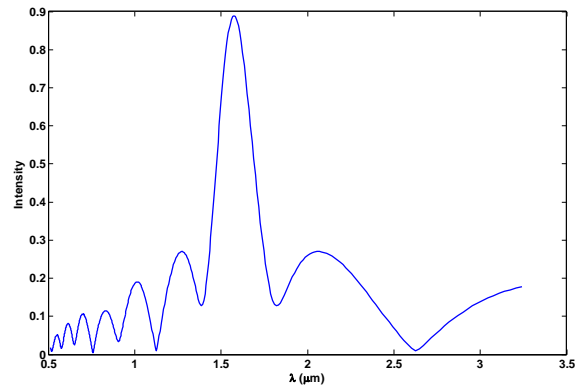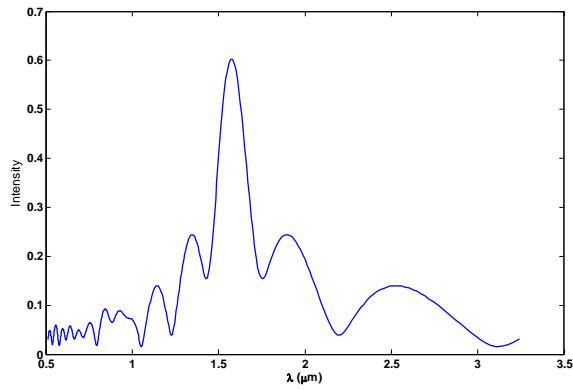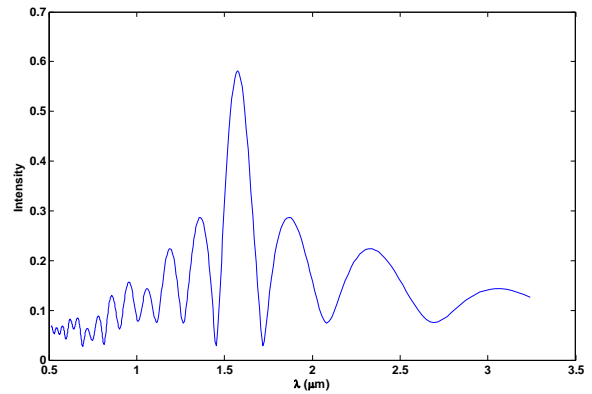
Figure 7.5. Wavelength response of cross channel output pulse of 9 mm PCF sample at a peak pulse power of: (a) 10KW (b) 50 KW (c) 75 KW and (d) 100 KW

Figure 7.6. Wavelength response of bar channel pulse propagation of 9 mm PCF coupler sample at a peak pulse power of: (a) 10KW (b) 50 KW (c) 75 KW and (d) 100 KW

Figure 7.7 Wavelength response of bar channel pulse propagation of 9 mm PCF sample at a peak pulse power of: (a) 10KW (b) 50 KW (c) 75 KW and (d) 100 KW

CHAPTER 8:   CONCLUSIONS

Linear and nonlinear characteristics of optical waveguide specifically the PCF were numerically studied here in this dissertation to overcome the limitation of existing analytical form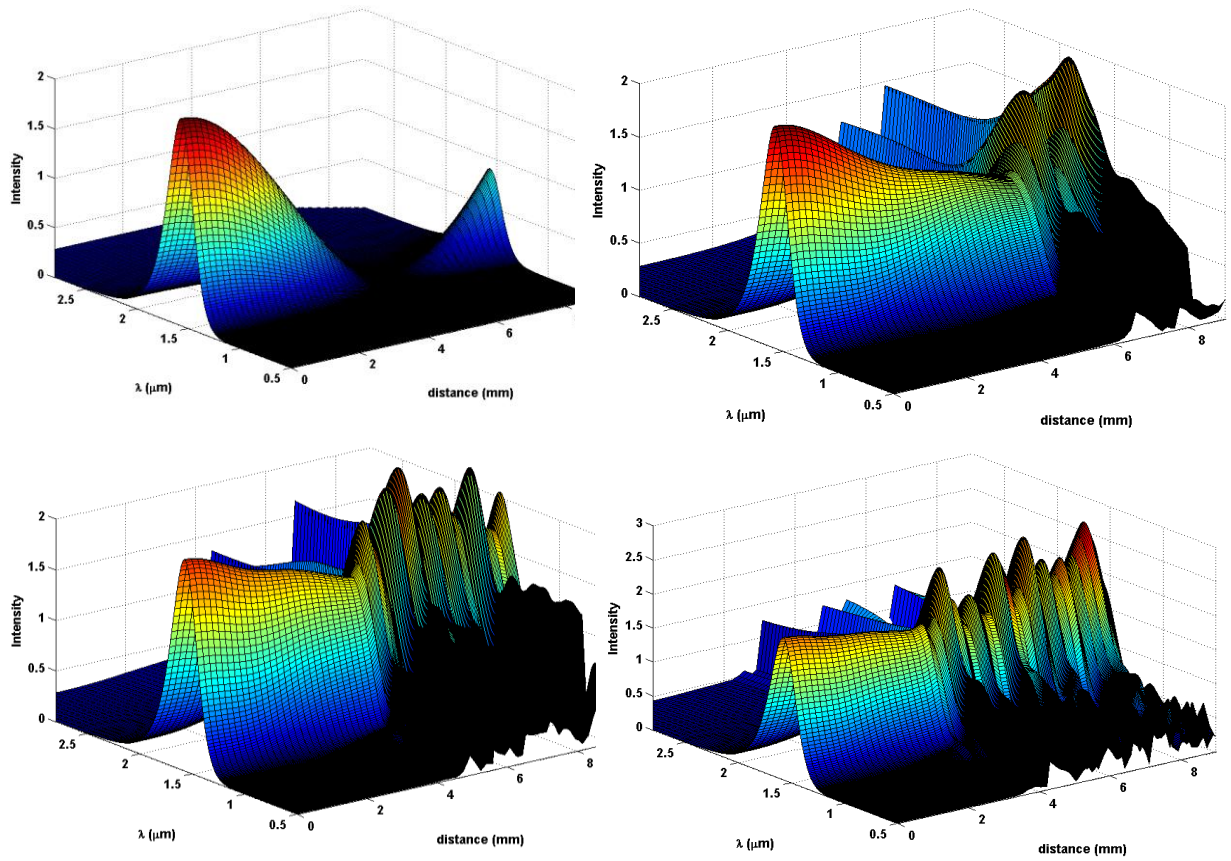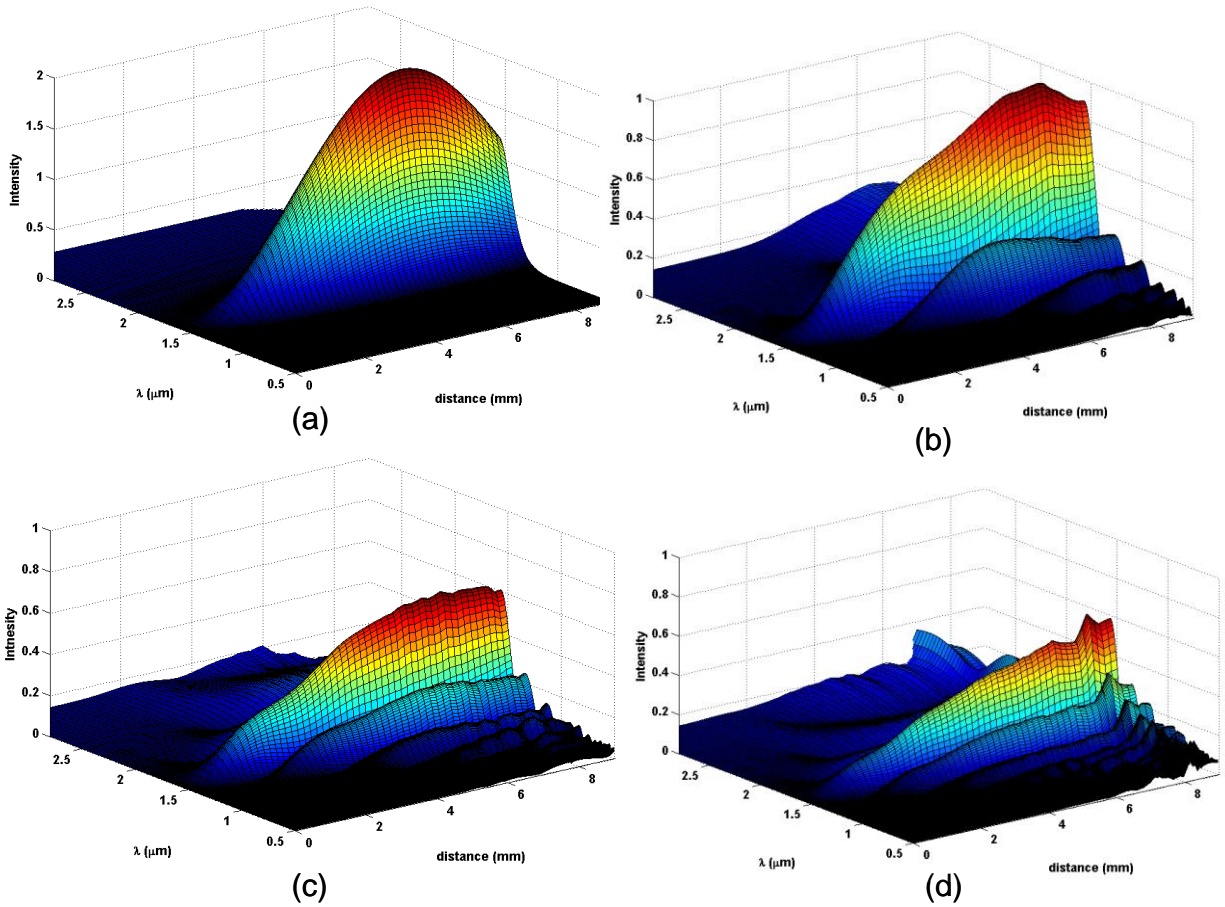ulation. We have built an edge vector element based FEM for the optical waveguide's modal analysis. Careful effort was made to avoid spurious/nonphysical solution. Field distribution with proper power normalization has been evaluated for the structures in order to incorporate the intensity dependent refractive index change in the waveguide material in our model. Accurate dispersion relation along with field distribution was investigated for the nonlinear pulse propagation.

The model also provides us the coupling characteristics of coupled waveguide structure. We evaluated the coupling coefficients of dual core PCF from the wave vector of even and odd modes over a wide wavelength range. The cladding structure, core diameter and core separation was innovatively adjusted to achieve desired coupling along with the dispersion characteristics. While designing this optical waveguide we found more degree of freedom in PCF than regular fiber.

This is the foundation to numerically investigate the nonlinear phenomenon observed in PCF such as self and cross phase modulation, scattering etc. Femtosecond pulse propagation was modeled by the coupled nonlinear Schrödinger equation and that equation was solved by using SSFM. Necessary term such as higher order dispersion, Raman scattering, SPM and XPM, self steepening (shock term) etc. was added in the equation in order to describe the physical effects. Effect of dispersion (GVD and TOD) along with the input power was reported. The results show how the pulse propagates at different wavelength.

Recently reported experimental results revealed some novel nonlinear phenomenon such as nonlinear switching and multi-wavelength generation in dual core PCF. Using our model numerically we demonstrated pulse switching which matches reasonably with the experimental results. Successful design effort was made in order to achieve appropriate PCF coupler parameters so that it can support soliton switching.

The nonlinear pulse propagation model reveals that at higher intensity the pulse energy spread into multiple frequencies primarily due to SPM. Frequency domain analysis shows that at higher input power the pulse starts spreading in to other frequencies as it propagates through the coupler. These observations help us understand the other spectral features observed in the experiment. It is evident that SPM is responsible for spectral broadening but some of the spectral peak observed at short wavelength was due to frequency mixing including existence of proper phase matching condition. SRS causes a 15 THz shifting of the pulse peak impulse.

REFERENCES

[1] G. P Agrawal, "*Nonlinear Fiber Optics*, 3rd *edition*", Academic press, (2001).

[2] R. W. Boyd, "*Nonlinear Optics*, 2nd *edition*", Academic Press, (2003).

[3] Y.R Shen, "*Principles of nonlinear optics*", Wiley, NY, (1984).

[4] P. Banerjee, "*Nonlinear optics: Theory, "Numerical Modeling and Applications"*, Mercel Dekker, Inc., (2004).

[5] J. Moloney and A. Newell, "*Nonlinear Optics*", Westview Presss, MA, (2004).

[6] *Handbook of Optics*, vol. 4, Optical Society of America, (2001).

[7] G. P Agrawal, "*Application of Nonlinear Fiber Optics*, 2nd *edition*", Academic press, (2001).

[8] Constantine A. Balanis, *Advanced Engineering Electromagnetics*, John Wiley & Sons, Inc.(1989).

[9] John L. Volakis, Arindam Chatterjee, Leo C. Kempel, "*Finite element method for electromagnetics: Antennas, Microwave Circuits, and Scattering Application*", Wiley-IEEE Press, (1998).

[10] K. Okamoto, "*Fundamentals of Optical Waveguides*", Academic Press, (2001).

[11] F.A. Fernandez and Y. Lu, "*Microwave and optical wave guide analysis by the finite element method*", John Wiley and Sons Inc. NY, (1996).

[12] J. Jin, "*The Finite Element Method in Electromagnetics*", J. Wiley & Sons (2002).

[13] A. Bjarkiev, J. Broeng, AS Bjarkiev, "*Photonic crystal fibers*", Kluwer Accedemic Publishers, (2003).

[14] J. C. Knight, "Photonic crystal fibres", Nature, **424**, 847-51, (2003).

[15] K. Yasumoto, *Electromagnetic theory and applications for the Photonic Crystals*, CRC Taylor & Francis, (2006).

[16] J. C. Knight, T. A. Birks, P. S. J. Russell and D. M. Atkin, "All-silica single-mode optical fiber with photonic crystal cladding", Optics Lett. 21 (19), pp.1547,(1996).

[17] T. A. Birks, J.C. Knight, and **P**.St.J. Russell, "Endlessly single-mode photonic crystal fibre", Optics Lett. 22 (13), p. 961, (1997).

[18] F. Benabid, J. C. Knight, G. Antonopoulos, P. St. J. Russell, "Stimulated Raman scattering in hydrogen-filled hollow-core photonic crystal fiber", Science 298, 399 (2002).

[19] J. K. Ranka, R. S. Windeler, and A. J. Stentz, "Visible continuum generation in air-silica microstructure optical fibers with anomalous dispersion at 800 nm", Optics Lett. 25 (1), p. 25, (2000).

[20] V. Ravi Kumar, A. George, W. Reeves, J. Knight, P. Russell, F. Omenetto, and A. Taylor, "Extruded soft glass photonic crystal fiber for ultra broad supercontinuum generation", Optics Express 10 (25), p.1520, (2002).

[21] A. Betlej, S. Suntsov, K. G. Makris, L. Jankovic, D. N. Christodoulides, G. I. Stegeman, J. Fini, R. T. Bise and D. J. DiGiovanni, "All-optical switching and multi-frequency generation in a dual core photonic crystal fiber," Optics Lett., **31**, pp.1480-1482, (2006).

[22] W. Jiang, L. Shen, D. Chen, and Hao Chi, "An Extended FDTD Method With Inclusion of Material Dispersion for the Full-Vectorial Analysis of Photonic Crystal Fibers" Journal of Light wave Technology, Vol. 23 (11), (2006).

[23] F. Fogli, L. Saccomandi, P. Bassi, G. Bellanca, and S. Trillo, "Full vectorial BPM modeling of index guiding photonic crystal fibers and couplers", Opt. Express, **10**, pp. 54-59, (2002).

[24] X. Wang, J. Lou, C. Lu, C. Zhao and W.T. Ang, "Modeling of PCF with Multiple Reciprocity Boundary Element", **12**, *Opt. Express*, pp. 961-966, (2004).

[25] K. Saitoh and M. Koshiba, "Numerical Modeling of Photonic Crystal Fibers," J. of Light Wave Tech., **23**, pp3580-3591, (2006).

[26] K. Saitoh and M. Koshiba, "Full-vectorial imaginary-distance beam propagation method based on a finite element scheme: application to photonic crystal fibers," IEEE J. Quantum Electron., vol. 38, pp. 927-933, (2002).

[27] Leader and Jeffery, "*J Numerical Analysis and Scientific Computation*", Addison Wesley, (2004).

[28] S.S. Sastry, "*Introductory methods of numerical analysis, 3rd edition*", Prentice Hall of India, (1999).

[29] Satish V. Blasubramaniam, "Finite Element Analysis of Left Handed Waveguide," MS thesis submitted to the school of electrical engineering and computer science, University of Central Florida, Fall (2004).

[30] J. S. Walker, "*Fast Fourier Transforms*", CRC Press, (1996).

[31] L.N. Trefethen, "*Spectral Methods in MATLAB*", SIAM, Philadelphia, (2000).

[32] C. J. Reddy, Manohar D. Desphande, C. R. Cockrell, and Fred B. Beck, "Finite element method for eigenvalue problems in electromagnetics," NASA Technical Paper, p. 3485, (1994).

[33] H.Whitney, "*Geometric Integration Theory*", Princeton University Press, (1957).

[34] J.C. Nedelec, "Mixed finite elements in R^3", Numer. Meth., vol. 35, pp. 315-341, (1980).

[35] M. Hano, "Finite-element analysis of dielectric-loaded waveguides," IEEE Trans. Microwave Theory Tech., vol. MTT-32, pp. 1275-1279, (1984).

[36] Mur and A. T. de Hoop."A finite-element method for computing three dimensional electromagnetic fields in inhomogeneous media", IEEE Trans. Magn., vol. MAG-21, pp. 2188-2191, (1985).

[37] M. Koshiba, "*Optical Waveguide Analysis,*" McGraw-Hill Publ., New York, 1992

[38] M. Sheik-Bahae, M. Sheik-Bahae, D. J. Hagan, and E. W. Van Stryland, "Dispersion and band-gap scaling of the electronic Kerr effect in solids associated with two-photon absorption", Phys. Rev. Lett. 65 (1), p. 96, (1990)

[39] S. N. Makarov, "*Antenna and EM Modeling with MATLAB*", Wiley-interscience, (2002).

[40] P. Kaiser and H. W. Astle, "Low-loss single-material fibers made from pure fused silica", Bell System Tech. J. 53, p.1021 (1974).

[41] P. St. J. Russell, "Photonic crystal fibers", Science 299, p. 358, (2003).

[42] T. A. Birks, P. Roberts, F. Couny, H. Sabert, B. Mangan, D. Williams, L. Farr, M. Mason, A. Tomlinson, T. Birks, J. Knight, and P. St. J. Russell, "Ultimate low loss of hollow-core photonic crystal fibers", Opt. Express 13 (1), p. 236 (2004).

[43] J. M. Fini, "Aircore microstructure fibers with suppressed higher-order modes", Opt. Express 14 (23), p.11354, (2006).

[44] H. Han, Park, M. Cho, and J. Kim, "Terahertz pulse propagation in a plastic photonic crystal fiber", Appl. Phys. Lett. 80 (15), p. 2634, (2002).

[45] Guobin Ren, Ping Shum, Liren Zhang, Xia Yu, Weijun Tong, and Jie Luo, "Low-loss all-solid photonic bandgap fiber", Optics Lett. 32 (9), p.1023, (2007).

[46] D. Mogilevtsev, T.A. Birks and P. St.J. Russell, "Group-velocity dispersion in photonic crystal fibres", Optics Lett. 23 (21), p.1662, (1998).

[47] R. F. Cregan, B. J. Mangan, J. C. Knight, T. A. Birks, P. St. J. Russell, P. J. Roberts, D. C. Allan, "Single-mode photonic band gap guidance of light in air", Science 285, p.1537, (1999).

[48] Knight, J.C.; Arriaga, J.; Birks, T.A.; Ortigosa-Blanch, A.; Wadsworth, W.J.; Russell, P.St.J., "Anomalous dispersion in photonic crystal fiber", Photon. Technol. Lett. 12, 807, (2000).

[49] J. C. Knight, T.A. Birks, R.F. Cregan, P.St.J. Russell and J.-P. de Sandro, "Large mode area photonic crystal fibre", Electron. Lett. 34, p.1347, (1998).

[50] A. Ortigosa-Blanch, J. C. Knight, W. J. Wadsworth, J. Arriaga, B. J. Mangan, T. A. Birks, and P. St. J. Russell, "Highly birefringent photonic crystal fibres", Optics Lett. 25 (18), 1325, (2000).

[51] K. Hougaard and F. D. Nielsen, "Amplifiers and lasers in PCF configurations", J. Opt. Fiber. Commun. Rep. 1, pp.63–83, (2004).

[52] C. Lin and R. Stolen, "New nanosecond continuum for excited-state spectroscopy", Appl. Phys. Lett. 28, p.216, (1976).

[53].K. Saitoh, Y. Sato, and M. Koshiba, "Coupling characteristics of dual-core photonic crystal fiber couplers", Opt. Express, **11**, pp. 3188-3195, (2003).

[54] Kaisar R. Khan, and Thomas Wu, "Finite Element Modeling of Dual Core Photonic Crystal Fiber" Accepted by ACES journal, (2008)

[55] Kaisar R. Khan and Thomas Wu, "Short Pulse Propagation in Wavelength Selective Index Guided Photonic Crystal Fiber Coupler", *IEEE Journal of Selected Topics in Quantum Electronics*, 14, pp.752-757, (2008).

[56] W. Sellmeier, *Annalen der Physik und Chemie*, 143, p. 271, (1871).

[57] J-P Goure and I Verrier, *Optical Fiber Devices*, IoP publication, MPG Books Ltd. UK, (2002).

[58] Fundamentals of Optical Fibers, Wiley inter series publication, John Wiley& Sons, Inc.,(1995).

[59] G. P. Agrawal, *Lightwave Technology: Components and Devices*, John Wiley& Sons, Inc., (2004).

[60] M. M. K. Liu, *Principle and Applications of Optical Communications*, Irwin, (1996).

[61] M. D Fleit and J. A. Fleck, "Light propagation in graded-index optical fibers," Applied optics 17, p.3990, (1978).

[62] K. Saitoh, M. Koshiba, T. Hasegawa, and E. Sasaoka, "Chromatic dispersion control in photonic crystal fibers: application to ultra-flattend dispersion," *Opt. Express*,11, pp. 843-852, (2003).

[63] K. Saitoh and M. Koshiba, "Imperical relations for simple design of photonic crystal fibers," *Opt. Express*,13, no.1 pp. 267-274, (2004).

[64] C. V. Raman and K. S. Krishnan, "A New Type of Secondary Radiation Nature," *121(3048)*, 501,(1928).

[65] Herzberg, "*Spectra of Diatomic Molecules*, Litton Educational Publishing," 1950

[66] A. Hasegawa and F. Tappert. "Transmission of stationary nonlinear optical pulses in dispersive dielectric fibers. I. Anomalous dispersion" Appl. Phys. Lett. Volume 23, Issue 3, pp. 142-144, (1973).

[67] L. Mollenauer and J. Gordon, "*Solitons in Optical Fibers: Fundamentals and Applications*", Accadmic Press, (2006).

[68] C.S Gardner, Jm. Green, M. D. Kruskal, and R. M. Miura, Physical Review Letter, 19, 1095, (1967).

[69] N. J. Jabusky and M. D. Kruskal Physical Review Letter, 15, 240, (1965).

[70] M.J. Ablowitz and P. A. Clarkson, *Soliton Nonlinear Evolution and Inverse Scattering*, Cabridge University Press, NY, (1991).

[71] G. H. Gu, *Soliton Theory and its Application*, Springler-Verlag, NY (1995).

[72] A. Hasegawa and F. Tappert, Applied Physics Letter, 23, p.142, (1973).

[73] M. J. Potasek and Y. Yang, "Multiterabit-per-second all-optical switching in a nonlinear directional coupler", IEEE J. Selected Topics in Quantum Electron, 8, pp. 714-721, (2002).

[74] P. Emplit, J.P. Hamaide, F. Reynaud, C. Froehly and A. Barthelemy, "*Picosecond steps and dark pulses through nonlinear single mode fibers*". Optics. Comm. 62, 374 (1987).

[75] Linn F. Mollenauer and James P. Gordon *Solitons in optical fibers.* Elsevier Academic Press, (2006).

[76] N. Manton and P. Sutcliffe (2004). *Topological solitons.* Cambridge University Press.

[77] Sulem Catherine and Sulem Pierre-Louis, "The Nonlinear Schroedinger Equation: Self-Focusing and Wave Collapse", Applied Mathematical Sciences 139, Springer-Verlag, (1999).

[78].R. S. Tasgal and M. J. Potasek, "Soliton solutions to coupled higher-order nonlinear Schroedinger equations", J. Math. Phys. 33, pp.1208-1215, (1992).

[79] S. Trillo, S. Wabnitz, E. M. Wright, and G. I. Stegeman, "Soliton switching in fiber nonlinear directional couplers," Optics Lett.., 13, pp. 672–674, (1988).

[80] Jean-Claude Diels, Wolfgang Rudolph, *Ultrashort Laser Pulse Phenomena: Fundamentals, Techniques, and Applications on a Femtosecond Time Scale*, Accadmic Press, (2006)

[81] J. Orear. Physik. Carl hansen Berlag., Munchen, Vienna, Austria, (1982)

[82] R. A. Serway, C. J. Moses, and C.A. Moyer, *Modern Physics*, Saunders College Pulblishers, Philadelphia, PA, (1989).

[83] R. Ramaswami and K. N. Sivarajan, *Optical Networks*, Morgan Kaufmann, San Francisco, (1998).

[84] B.J. Mangan, J.C. Knight, T.A. Birks, P.St.J. Russell, and A.H. Greenaway, "Experimental study of dualcore photonic crystal fibre," *Electron. Lett*.,36, pp. 1358-1359, 2000.

[85] Kaisar R. Khan, Thomas X. Wu, Demitrios N. Christodoulides and George I. Stegeman, "Soliton Switching and Multifrequency generation in Nonlinear Photonic Crystal Fiber" Optics Express, 16(13), pp.9417-9428, May 2008.

[86] J. Dudley, Goëry Genty and Stéphane Coen,"Supercontinuum generation in photonic crystal fiber", Rev. Mod. Phys. 78, p.1135, (2006).

[87] R. R. Alfano and S. L. Shapiro, "Observation of self-phase modulation and small-scale filaments in crystals and glasses", Phys. Rev. Lett. 24 (11), pp.592, (1970).

[88] M. Bellini and T. W. Hänsch, "Phase-locked white-light continuum pulses: toward a universal optical frequency comb synthesizer", Opt. Lett. 25 (14), pp.1049, (2000).

[89] J. M. Dudley et al., "Super continuum generation in air-silica microstructure fibers with nanosecond and femtosecond pulse pumping", J. Opt. Soc. Am. B 19 (4), p.765 (2002).

[90] W. J. Wadsworth, A. Ortigosa-Blanch, J. C. Knight, T. A. Birks, T.-P. Martin Man, and P. St. J. Russell, "Super continuum generation in photonic crystal fibers and optical fiber tapers: a novel light source", J. Opt. Soc. Am. B 19 (9), 2148 (2002)

[91] S. Coen, A.H. L. Chau, R. Leonhardt, J.D. Harvey, J.C. Knight, W.J. Wadsworth, and P. St. J. Russell, "Super continuum generation by stimulated Raman scattering and parametric four-wave mixing in photonic crystal fibers", J. Opt. Soc. Am. B 19 (4), pp.753-763 (2002).

[92] A. V. Gorbach and D. V. Skryabin, "Light trapping in gravity-like potentials and expansion of super continuum spectra in photonic-crystal fibres", Nature Photonics 1, p.653 (2007).